AFIT/GAE/ENY/90D-07

AD-A230 826

BIFURCATION ANALYSIS OF THE LONGITUDINAL DYNAMICS OF A SIMPLE POWERED LIFTING HYPERSONIC VEHICLE

THESIS

Eric E. Fox
Captain, USAF

AFIT/GAE/ENY/90D-07

DTIC
ELECTE
JAN 09 1991
D

Approved for public release; distribution unlimited

91 1 3 090

This document has been approved for public release and sale; its distribution is unlimited.

AFIT/GAE/ENY/90D-07

BIFURCATION ANALYSIS OF THE LONGITUDINAL DYNAMICS OF A SIMPLE POWERED LIFTING HYPERSONIC VEHICLE

THESIS

Eric E. Fox
Captain, USAF

AFIT/GAE/ENY/90D-07

DTIC
ELECTE
JAN 09 1991
D

Approved for public release; distribution unlimited

AFIT/GAE/ENY/90D-07

BIFURCATION ANALYSIS OF THE LONGITUDINAL DYNAMICS OF A SIMPLE POWERED LIFTING HYPERSONIC VEHICLE

THESIS

Presented to the Faculty of the School of Engineering

of the Air Force Institute of Technology

Air University

In Partial Fulfillment of the

Requirements for the Degree of

Master of Science in Aeronautical Engineering

Eric E. Fox, B.S.

Captain, USAF

December 1990

Accession For	
NTIS GRA&I	X
DTIC TAB	☐
Unannounced	☐
Justification	
By	
Distribution/	
Availability Codes	
Dist	Avail and/or Special
A-1	

Approved for public release; distribution unlimited

Preface

The purpose of this study was to investigate the nonlinear behavior of a simple powered lifting hypersonic vehicle flying in a near circular orbit above a spherical nonrotating Earth with gradients in atmospheric density and pressure and an inverse square law for gravity. The vehicle is constrained to fly in a vertical plane so only longitudinal motion is modeled. Bifurcation analysis, utilizing the AUTO software package, was used to conduct this study. A simple five-state model with three different thrust laws was used to describe an unaugmented vehicle whose geometric and aerodynamic characteristics follow those of the literature. A parameter represented a body flap deflection (δ_{bf}) was used to conduct one set of bifurcation sweeps for each thrust law. Then a second set of bifurcation sweeps for each thrust law was obtained using a parameter representing a throttle (δT) which scaled the value of the thrust. Secondary parameters representing simple feedback gains, were subsequently added.

I wish to extend my sincerest thanks to my thesis advisor, Capt Jim Planeaux, for his patient and caring nature. His guidance and insight were invaluable. I would also like to thank the members of my thesis committee, Dr. Brad Liebst and Major Curtis Mracek for their comments while reviewing this document. Finally, but most importantly, I would like to thank my dearest friend and love, Cynthia, for always being there for me and shouldering the responsibilities of our family during my time at AFIT.

Eric E. Fox

Table of Contents

Page

List of Figures

Figure Page

List of Tables

Notation

α : angle of attack (radians)

δ_{bf} : body flap deflection (degrees)

δ_{bfc} : commanded body flap deflection (degrees)

δT : throttle parameter

Δ : perturbation quantity

γ : flight path angle (radians)

λ : parameter for example problem (=F/mg)

μ : longitude (radians), also eigenvalue

θ : pitch angle (radians)

ρ : density (slug/cu ft)

ω^{bi} : angular velocity of body frame to inertial frame (radians/sec)

ω^{E} : angular velocity of Earth (radians/sec)

ω^{vi} : angular velocity of vehicle carried frame to inertial frame (radians/sec)

ω^{wi} : angular velocity of wind frame to inertial frame (radians/sec)

An : area of exhaust nozzle (ft^2)

a : acceleration ($ft - sec^{-2}$)

C_D : drag coefficient

C_{D0} : basic drag coefficient

$C_{D\alpha}$: partial derivative of drag w.r.t. angle of attack (1/radian)

C_L : lift coefficient

C_{L0} : lift coefficient at zero angle of attack

$C_{L\alpha}$: partial derivative of lift w.r.t. angle of attack (1/radian)

C_m : pitching moment coefficient

C_{m0} : basic pitching moment

$C_{m\delta bf}$: partial derivative of pitching moment w.r.t. body flap deflection (1/deg)

$C_{m\alpha}$: partial derivative of pitching moment w.r.t. angle of attack (1/radian)

C_{mq} : partial derivative of pitching moment w.r.t. pitch rate (sec/radian)

D : drag (lb)

F : force generated by constant torque (F=T/r) in example problem (lb)

g(r) : gravity as a function of radius from Earth's center ($ft - sec^{-2}$)

h : altitude (ft)

k_0 : $(I_x - I_z)/I_y$

k_y : radius of gyration in pitch (ft)

K_q : pitch rate feedback gain

l : characteristic length (vehicle length) (ft)

L : lift (lb)

m : mass (slugs)

M : sum of moments about vehicles center of mass (ft - lb)

M : Mach number

Pa : ambient pressure (psf)

Pe : nozzle exit pressure (psf)

q : pitch rate of vehicle relative to Earth (radian/sec)

q_0 : pitch rate relative to the Earth at starting altitude (radian/sec)

r : geocentric radius (ft), also length of rod in example problem (ft)

s : area of lifting surface (ft^2)

T : thrust (lb), Period (seconds), torque (ft-lb)

V : velocity (ft/sec)

Vexh : rocket nozzle exhaust velocity (ft/sec)

W : weight (lb)

X_r : partial derivative of the longitudinal force w.r.t. radius

X_u : partial derivative of the longitudinal forces w.r.t. velocity in the $\hat{w}_x$ direction

$()_e$: equilibrium value; also value for example problem (i.e. θ_e)

$()_0$: values at initial starting equilibrium solution

$(\dot{})$: derivative with respect to time

(I_x, I_y, I_z) : moments of inertial about body axes (slug - ft^2)

$(\hat{i}, \hat{j}, \hat{k})$: unit vectors for the inertial frame

$(\hat{b}_x, \hat{b}_y, \hat{b}_z)$: unit vectors for the body fixed frame

$(\hat{v}_x, \hat{v}_y, \hat{v}_z)$: unit vectors for the vehicle carried frame

$(\hat{w}_x, \hat{w}_y, \hat{w}_z)$: unit vectors for the wind axis frame

Abstract

Bifurcation analysis was used to investigate the nonlinear behavior of a simple powered lifting hypersonic vehicle in circular orbit about a spherical nonrotating Earth with gradients in atmospheric density and pressure and an inverse square law for gravity. Vehicle motion is constrained to a vertical plane so only longitudinal dynamics were modeled. Bifurcation analysis was conducted using the AUTO software package. A simple five-state model with three different thrust laws was derived to describe an unaugmented vehicle whose geometric and aerodynamic characteristics follow those of the literature. A parameter representing a body flap deflection (δ_{bf}) was used to conduct one set of bifurcation sweeps for each thrust law. A second set of bifurcation sweeps for each thrust law was obtained using a parameter representing a throttle (δT) which scaled the thrust. Secondary parameters representing simple feedback gains were subsequently added. Results were surprising for a simple system with basically linear aerodynamics. Periodic branches arising from the loss of pitch stability or associated with a "resonance altitude" are routinely found with significant amplitude, and periods on the order of an elliptical orbit's period for a given geocentric radius. Rotational states generally had sub-oscillations of greater frequency.

BIFURCATION ANALYSIS OF THE LONGITUDINAL DYNAMICS OF A SIMPLE POWERED LIFTING HYPERSONIC VEHICLE

I. Introduction

Introductory Discussion

In the past interest in hypersonic vehicle dynamics has concentrated on assuring stable reentry and return to a few specific points on the earth. The need for maneuverability was limited. The renewed interest in lifting hypersonic vehicle dynamics and design; brought about by the Trans-Atmospheric Vehicle projects, Boost Glide Vehicles, the National Aerospace Plane and other hypersonic lifting vehicles designed for improved maneuverability and greater versatility; has generated a need to better understand and anticipate their possible nonlinear dynamic effects. Specifically, the ability to predict nonlinear dynamic responses, periodic equilibrium states and other dynamic phenomena for a representative hypersonic vehicle is growing in importance. Previous work by Etkin (4), Berry (2), Vihn (15) and others demonstrate some interesting behavior of the longitudinal dynamics for hypersonic vehicles due to the variation of atmospheric density, gravity and Mach number with altitude. Bifurcation and continuation analyses have been used successfully to examine the nonlinear behavior of fighter aircraft in a variety of configurations. It was felt this type of analysis would yield insight into the nonlinear behavior of a hypersonic vehicle as well.

The purpose of this thesis was to explore the nonlinear dynamic responses of a hypersonic vehicle and using a more global technique to investigate these effects. In addition, it is hoped the application of bifurcation analysis techniques to the highly nonlinear hypersonic regime would help extend the basic techniques available for further analysis of hypersonic vehicles.

Summary of Previous Studies

Several papers have been presented over the last four decades that impact directly on the study of the longitudinal dynamics of a hypersonic vehicle flying in an atmosphere that contains gradients in density and the effects of curvature of the flight path. Most of these previous works built in some way upon the work presented in 1950 by Neumark (9), which was then extended to a lifting vehicle in orbital flight by Etkin (4) in 1961. The results of these later works have served to enhance the material originally found in these two landmark papers for lifting vehicles. Having said this one should note that some correction of Etkin's observations regarding the behavior of the phugoid and pitching mode characteristics are found in the work by Vihn and Dobrzelecki (15) and verified in a later paper by Markopoulos, et al (7) as well as this author's most recent work.

In his paper Neumark details the motivation for his work which was based on several of the very first studies of the behavior of airplanes in steep angled dives. He is one of the original writers on the subject of the effect of density gradients on airplanes having published his first work on the subject in 1931; the earliest being in 1929. His paper

published in 1950 was the first published work in which the longitudinal equations of motion were cast in the form of a quintic; having added an equation to describe the change in altitude with time. This form of the longitudinal equations gives rise to a fifth, real root (eigenvalue) which gives an indication of the vehicles ability to hold a fixed equilibrium altitude. The results of his study demonstrate the increasing affect the density gradient has on the longitudinal dynamics as the speed of the vehicle approaches Mach one. Neumark found that the principal effect of the density gradient is on the phugoid mode; he states that the short period (pitching) mode is unaffected. Increasing density, increases the phugoid frequency thus shortening the period. The effect on phugoid damping was not clear having been complicated by compressibility effects at speeds above $M = 1.4$. He concluded the height mode would have a very long time constant and may be either a subsidence or divergence and has importance only for hypersonic flight or flight at constant altitude for long periods of time (9:325).

Etkin's classic of 1961 extends Neumark's work to the truly hypersonic case and includes, necessarily, the mathematical modifications to account for the curvature of the undisturbed flight path and the variation of gravity with altitude. In his analysis the longitudinal equations of motion for flight in a vertical plane about a nonrotating Earth whose atmosphere is at rest are linearized and the behavior of the vehicle subject to small disturbances about an equilibrium is examined. In addition, he presents results from numerical solutions to the nonlinear equations and does a comparison with the linear approximation. Of note in the equations of motion is the addition of the torque about the vehicle's center of mass due to the small variation of gravity acting on a body at

very high altitudes (above 500,000 ft) where the pitch damping is negligible. In this realm the gravity torque generates the dominant moment acting on the vehicle and for a standard vehicle configuration whose longitudinal axis is nearly aligned with the flight path this effect is destabilizing.

Etkin examines four basic cases using the same (steady reference) lift coefficient ($C_L = 0.05$ [rad^{-1}]).

Case A Constant thrust rocket, full set of equations
Case B Air-breathing engine ($T \propto \rho$), full set of equations
Case C Approximate equations (i.e. no density gradient)
Case D Constant thrust rocket with $q_0 = 0$

where q_0 is the equilibrium value of the pitch rate relative to the Earth.

Etkin determined that the effects of varying density and gravity with altitude and the effects due to the Earth's curvature and the thrust law have significant impact on the phugoid mode and the stability of the height mode, but insignificant effect on the pitching (short period) mode except at very high altitude where the pitch damping is overcome by the gravity torque. In addition, Etkin found that above 400,000 ft the period of the pitching and phugoid modes approached each other and he asserts that they become equal, after which the phugoid tends toward the orbital period and the pitching mode tend toward infinity. In this altitude range he demonstrated a dynamic coupling between the two modes and when nearly equal all relation to two classical modes breaks down with substantial pitching motion in the phugoid mode. Finally when the two modes are exactly equal he determines the system to be unstable. For the height mode Etkin found that it represents "a spiral, proceeding away from the reference orbit." He also noted an interesting variation in the way the speed changes with altitude above and below 350,000 ft. Above this

altitude as the altitude is decreased the speed increases whereas below this altitude the opposite is the case (4:787-788).

In the work by Vihn and Dobrzelecki (15) an "analytic study of the longitudinal dynamics of a thrusting, lifting orbital vehicle in a nearly circular orbit" is conducted. The basic set of five equations used to describe the longitudinal motion of a vehicle in orbit about a spherical Earth were used. A strictly linear analysis as well as analysis including second order terms in the Taylor series expansion of the atmospheric density were used to develop explicit relationships to describe the orbital motion. Also developed were analytic expressions for the period and damping of the "angle of attack" (pitching) mode. As with Etkin they observed an altitude where the velocity-altitude relationship inverts. They went on to develop an expression based on vehicle characteristics that defines the altitude where this "inversion" takes place. Finally they found the trend at high altitude of the linearized phugoid or long-period mode and angle of attack (pitching) mode tend to become nearly equal in frequency, period and damping, then diverge. (Figure 1) Similar behavior for the very same equations was found earlier by Etkin (4:785-788) where he concluded the two modes "crossover" and the phugoid period tended to the orbital period while the period of the pitching (short period) mode tended toward infinity. At the point of "crossing" Etkin concluded the dynamic system would be unstable (4:787).

Stengel also found the same basic trends in the three longitudinal modes however his work looked more closely at the stability questions and dealt at some length with various techniques to provide altitude stability for a vehicle in supersonic cruising flight (13). In his work he uses the linearized equations for longitudinal motion, characterized by the

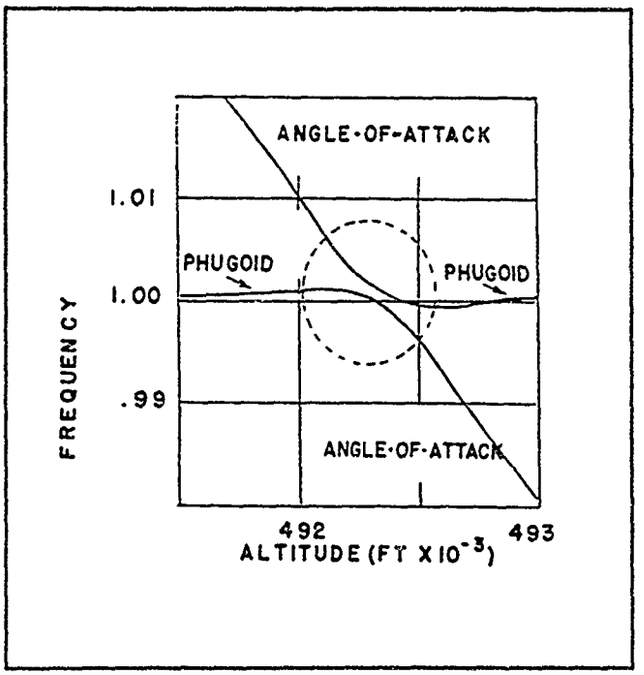

Figure 1. Frequencies near Resonance Altitude (15:19)

perturbation variables Δu (forward velocity), Δα (angle of attack), Δθ (pitch attitude), and Δh (altitude), to study the interrelations of motions these variable characterize. He then used this information to test how various combinations of feedback and control would affect altitude stability. In addition to developing analytical transfer functions he conducted numerical studies and summarizes the effectiveness of the various techniques proposed. Some of his results were tabulated in his work and are reproduced on the following page in Table 1.

In a later work by Berry (2), he examined the effect on the "long-period dynamics" of a vehicle of similar characteristics to previous authors but included an "advanced air-breather" with a more complicated thrust law which is more representative of a true hypersonic vehicle like the National Aerospace Plane. He concluded that the height mode stability and long-period damping were strongly affected by the slope of thrust with

Mach number (6:255-257). While all the trends indicated in his work are valid they are not in the strictest sense complete. It is the variation of the difference between thrust and drag with height and Mach number that determines stability. These more complete relations are identified in works by Markopoulos, et al (7:285) and Stengel (13:468,472). Berry further examined the effectiveness of various simple feedback schemes involving only the pitch control surface to stabilize the long-period and/or height modes. Some results for feeding back combinations of pitch attitude, forward velocity and altitude to the pitch control surface for the rocket and "advanced air-breather" were presented (2:256-257).

Most recent is the work by Markopoulos, Mease and Vihn (7) where the linearized equations of motion are used to examine the thrust law effects on the longitudinal dynamics of an aerospace vehicle flying at hypersonic speeds. Their work demonstrates the dependence of the height mode stability and phugoid damping on the way the longitudinal force varies with both altitude and speed. In addition they confirm the results of the previous study by Vihn and Dobrzelecki (15) for the high altitude trend of the phugoid or long-period mode and angle of attack (pitching) mode.

Of special interest in the work by Markopoulos, et al, is the characterization of expected height mode stability and phugoid damping over the plane of all thrust possibilities. The plane is defined by two parameters, specifically the variation in the longitudinal force with height (X_T) and velocity (X_V). The correlation of the points relating to earlier work by Etkin (4) are in excellent agreement. They went on to conclude that it is actually "the partial derivatives of the difference between thrust and drag with respect to speed and altitude that plays the key role in determining the stability of the translational dynamics (7:287)."

TABLE 1

SOME FEEDBACK EFFECTS FOR STENGEL'S STANDARD CASE WITH AUGMENTED SHORT PERIOD (FEEDBACK IS NEGATIVE UNLESS DENOTED BY (+))

Feedback Variable and Control	Height Mode	Phugoid Mode
Attitude to:		
thrust	SS	SI
lift (-)	I	S
lift (+)	SS	I
moment (-)	S	I
moment (+)	SI	S
Pitch angle to:		
thrust	N	I
lift (-)	I	SS
lift (+)	N	SI
moment (-)	I	SS[a]
moment (+)	N	SI
Forward Velocity to:		
thrust	SS	SS[a]
lift (-)	SI	SS
lift (+)	N	SI
moment	SS	SS[a]
Angle of attack to:		
thrust	N	SS
lift (-)	SI	SI[a]
lift (+)	N	SS
moment (-)	?	I
moment (+)	?	SS[b]

S = Stability SS = Strong Stability
I = Instability SI = Strong instability
N = Neutral stability
[a] With Limited Travel.
[b] Conditional Stability

Stengel (13:470)

This same relationship was discussed by Stengel in his article on "Altitude Stability for Supersonic Cruising Flight" (13:468,472). Markopoulos, et al, further concluded after numerical simulation of their full and reduced order mathematical models that over the plane of all engine possibilities

> "*if thrust increases faster than drag with respect to speed at least one of the translational modes (height or phugoid) will be unstable. Increasing the partial derivative of the differ-*

ence between thrust and drag with respect to altitude has a destabilizing effect on the height mode and a stabilizing effect on the phugoid (7:287)."

Finally, they concluded that to first order, the period of the phugoid mode as well as all characteristics of the pitching mode are independent of the thrust law (7:287).

Outline of Analysis

In this thesis the dynamic behavior of a powered lifting hypersonic vehicle in nearly circular orbital flight about the center of mass of a spherical nonrotating planet (specifically the Earth) whose atmosphere contains gradients in density and pressure and whose gravitational field follows the inverse square law is examined.

Throughout this thesis emphasis is given to the leading order aerodynamic behavior and simplifying assumptions to this end are brought to the readers attention as required. In order to focus the scope of this work it is assumed the flow is inviscid therefore the effects of high temperature gas flows are neglected. This assumption is consistent with general longitudinal analysis found routinely in the literature and allows use of simple Newtonian impact theory as the basis for the aerodynamics.

To begin this study the reader should have a good mental image of the problem being analyzed, and a well developed understanding of the equations used to describe the translation and rotation of a body flying a great circle about a spherical planet. To facilitate this the basic equations for a vehicle flying in an atmosphere at rest relative to a nonrotating spherical planet (ω^B=0) are derived. The first step in analyzing this problem is to identify an inertial reference frame. Then,

three advantageous frames of reference relative to the inertial frame are introduced from which a set of equations describing the forces and moments acting on the body of interest are developed. It is common in trajectory analysis to use a wind axis system as shown in Figure 2 where the positive x-axis is parallel to, but opposite, the relative wind. In this way the aerodynamic forces are cleanly defined and the velocity vector has a single non-zero component. For the analysis of angular momentum the body-fixed axes are used, also shown in Figure 2 as b_x and b_z, thus the moments of inertia are time invariant and for a fixed mass and mass distribution, as is the case here, the moments of inertia are constant. The vehicle axes indicated in Figure 2 by $(v)_{x,z}$ is used as a convenient intermediate frame between the body or wind axes and the inertial axes.

As with linear analysis, the bifurcation analysis begins at a known equilibrium point, but rather than linearizing the equations and looking at small disturbances about this point, a continuation method is used to solve for the flow of equilibrium solutions (specifically the pseudo-arc length technique resident to AUTO; the software package used for continuation and bifurcation analysis in this study) (3:12-16; 12:116). From the path of equilibrium solutions (or stationary points) bifurcating solutions, or in other words, additional solution paths are located and explored. Of the various types of possible solution branches special interest is given to branches obtained subsequent to a nonhyperbolic or degenerate point (12:18-20). These often give rise to branches of periodic solutions where motion, such as periodic oscillations develop. On these branches the dynamic behavior comes to life. Many of these concepts are clarified in section II where the nature of bifurcation analysis is discussed.

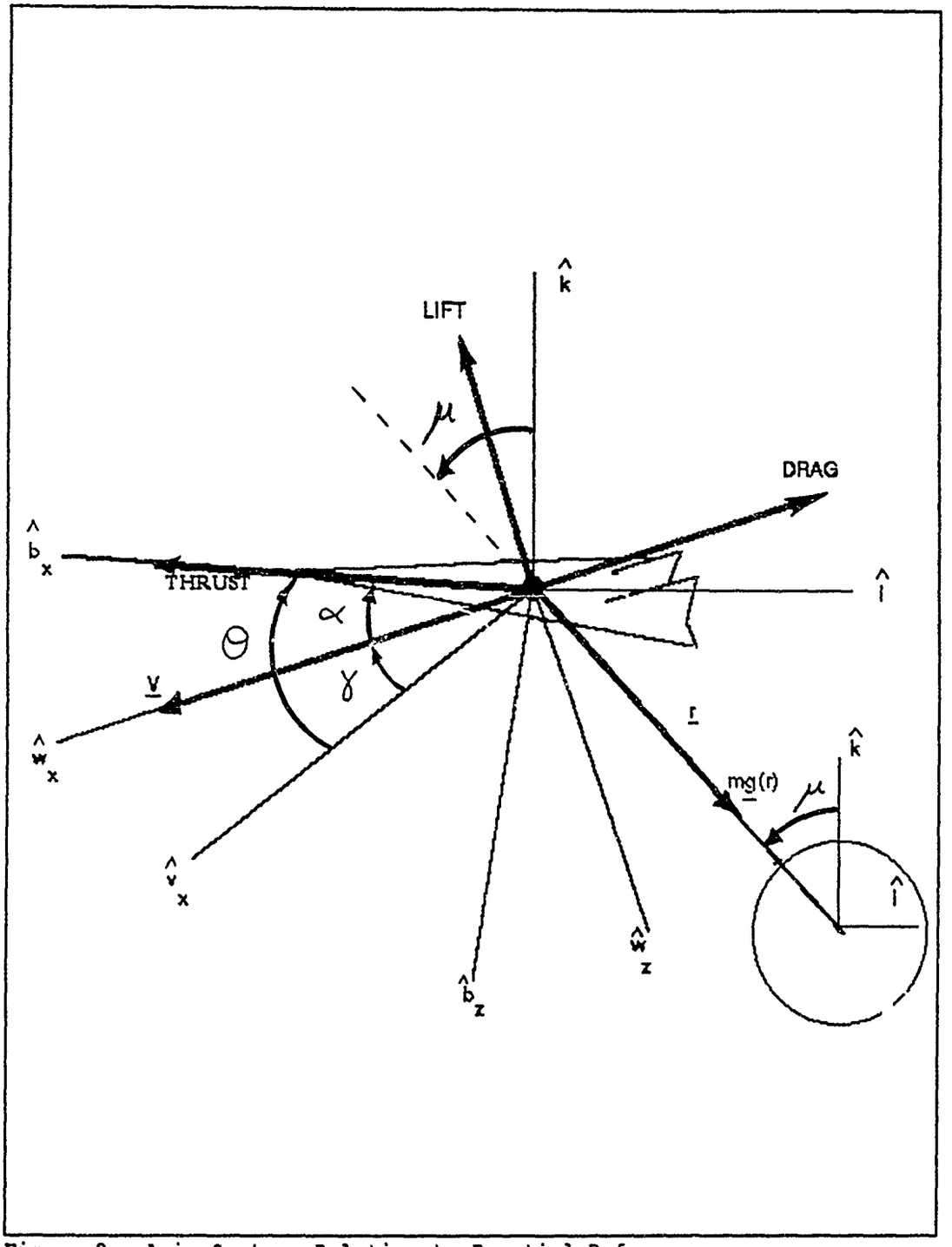

Figure 2. Axis Systems Relative to Inertial Reference

Equations of Motion

The author is indebted to Planeaux (10), McRuer, et al (8:204,220) and Etkin (5:104,148) for background and guidance for the following development. The reader is encouraged to review the two texts for details on the development of the following system of equations. To begin, the basic assumptions on which the equations of motion are based must be stated:

1. *The Earth is an inertial reference frame.*
2. *The vehicle is a rigid body.*
3. *The vehicle mass and mass distribution are constant.*
4. *The vehicle is symmetric about the x-z plane.*
5. *The body fixed axes are aligned with the principal axis of the vehicle.*

In addition to the simplifications resulting from the assumptions above, the terms associated with motion in the horizontal plane are neglected leaving the system as shown above in Figure 2.

Looking first at the angular and kinematic relations, by inspection the following angular rate of the three reference frames relative to the inertial frame are given as:

$$\underline{\omega}^{bi} = q\hat{j} = (-\dot{\mu} + \dot{\theta})\,\hat{j} = (\dot{\theta} + -\dot{\mu})\,\hat{B}_y \qquad (1)$$

$$\underline{\omega}^{vi} = (-\dot{\mu})\,\hat{j} = -\dot{\mu}\,\hat{v}_y \qquad (2)$$

$$\underline{\omega}^{wi} = (-\dot{\mu} + \dot{\gamma})\,\hat{f} = (\dot{\gamma} - \dot{\mu})\,\hat{w}_y \tag{3}$$

where:

$(\hat{i}, \hat{j}, \hat{k})$	=	unit vectors of inertial frame
$(\hat{b}_x, \hat{b}_y, \hat{b}_z)$	=	unit vectors of body frame
$(\hat{w}_x, \hat{w}_y, \hat{w}_z)$	=	unit vectors of wind frame
$\dot{\mu}$	=	time rate change of longitude (rad/sec)
$\dot{\gamma}$	=	time rate change of flight path angle (rad/sec)
$\dot{\theta}$	=	time rate change of pitch angle (rad/sec)
$\underline{\omega}^{bi}$	=	angular velocity of body to inertial frame (rad/sec)
$\underline{\omega}^{vi}$	=	angular velocity of vehicle to inertial frame (rad/sec)
$\underline{\omega}^{wi}$	=	angular velocity of wind to inertial frame (rad/sec)
q	=	pitch rate of the vehicle relative to the Earth (rad/sec)

The radius (r) is the distance from the center of mass of the Earth to the vehicles center of mass and written as a vector in the vehicle frame is given as:

$$\boldsymbol{r} = -r\hat{v}_z \tag{4}$$

where:

$(\hat{v}_x, \hat{v}_y, \hat{v}_z)$	=	unit vectors of the vehicle frame
r	=	geocentric radius (ft)

From eqn(4) the velocity can be written by differentiating in the vehicle frame:

$$\begin{aligned} \boldsymbol{V} = \dot{\boldsymbol{r}} &= -\dot{r}\hat{v}_z + \underline{\omega}^{vi} \times \boldsymbol{r} \\ &= -\dot{r}\hat{v}_z + \dot{\mu} r \hat{v}_x \end{aligned} \tag{5}$$

where:

γ	=	flight path angle (rad)
V	=	velocity (ft/sec)

However the velocity can also be shown to be:

$$\mathbf{V} = V(\cos(\gamma)\hat{v}_x - \sin(\gamma)\hat{v}_z) \tag{6}$$

By combining eqn(5) and eqn(6) the following scalar kinematic relations are obtained:

$$\dot{r} = V\sin(\gamma) \tag{7}$$

$$\dot{\mu} = \frac{V}{r}\cos(\gamma) \tag{8}$$

where: γ = flight path angle (rad)
r = radius (ft)
V = velocity (ft/sec)

From eqn(1) the equation for the time rate change of pitch angle can be obtained by solving for $\dot{\theta}$ as follows:

$$\dot{\theta} = q + \dot{\mu} \tag{9}$$

Following directly from the assumptions 3 through 5 the time rate change of the pitch velocity of the vehicle is given as (4:145):

$$\dot{q} = \frac{M}{I_y} \tag{10}$$

where: I_y = moment of inertia about the y-axis of the body (slug-ft^2)
M = sum of moments about the vehicle's center of mass (ft-lb)

Equations (7,9 and 10) make up three of the five equations of motion. The remaining two equations fall out of the force balance which is dealt with next.

Summing forces acting at the vehicles center of mass yields:

$$\begin{aligned} \boldsymbol{F} = m\boldsymbol{a} &= mg(r)\hat{V}_z + T\hat{b}_x - L\hat{w}_z - D\hat{w}_x \\ &= [-mg(r)\sin(\gamma) + T\cos(\alpha) - D]\hat{w}_x \\ &\quad + [mg\cos(\gamma) - T\sin(\alpha) - L]\hat{w}_z \end{aligned} \tag{11}$$

where:

a	=	acceleration (ft-sec^{-2})
D	=	drag (lb)
g(r)	=	gravity as a function of geocentric radius (ft-sec^{-2})
L	=	lift (lb)
m	=	mass (slug)
r	=	geocentric radius (ft)
T	=	thrust (lb)

Now velocity in the wind frame is written as $\boldsymbol{V}=V\hat{w}_x$. The acceleration in the wind frame is given by:

$$\dot{\boldsymbol{V}} = \boldsymbol{a} = \dot{V}\hat{w}_x - (\dot{\gamma}-\dot{\mu})V\hat{w}_z \tag{12}$$

Since $\boldsymbol{F}=m\boldsymbol{a}$ eqn(12) and eqn(11) can be set equal, after multiplying eqn(12) by the mass m, and upon separating into scalar components yields the following two equations.

$$m\dot{V} = T\cos(\alpha) - D - mg\sin(\gamma) \tag{13}$$

$$-m(\dot{\gamma} - \dot{\mu})V = -T\sin(\alpha) - L + mg\cos(\gamma) \tag{14}$$

Utilizing the relation $\dot{\theta} = \dot{\gamma} + \dot{\alpha}$ and eqn(9) the following expression is obtained:

$$q-\dot{\alpha} = \dot{\gamma}-\dot{\mu} \tag{15}$$

Substituting eqn(15) into the left hand side of eqn(14) and solving for $\dot{\alpha}$ yields the final equation for the set of five equations of motion.

$$\dot{\alpha} = q - \frac{T}{mV}\sin(\alpha) - \frac{L}{mV} + \frac{g(r)}{r}\cos(\gamma) \qquad (16)$$

Equations (7,9,10,13 and 16) comprise the set of five dynamic and kinematic equations for this analysis. Together with the following expressions for the aerodynamic forces and moments, and the thrust equations they comprise the complete set of equations required to conduct this study. The five equations of motion are reprinted below for convenience:

$$m\dot{V} = T\cos(\alpha) - D - mg\sin(\gamma) \qquad (13)$$

$$\dot{\alpha} = q - \frac{T}{mV}\sin(\alpha) - \frac{L}{mV} + \frac{g(r)}{r}\cos(\gamma) \qquad (16)$$

$$\dot{\theta} = q + \dot{\mu} \qquad (9)$$

$$\dot{q} = \frac{M}{I_y} \qquad (10)$$

$$\dot{r} = V\sin(\gamma) \qquad (7)$$

Aerodynamic Forces and Moment Coefficients. As with linear analysis the standard forms of the forces and the moment due to aerodynamics will be used, and are listed below. Notice however, the term on the right hand side of eqn(19). This term is the moment about the center of mass of a satellite in a gravitational field and as found by Etkin is a significant

factor at high altitudes (4:783; 11:21).

$$D = \frac{1}{2}\rho V^2 S C_D \tag{17}$$

$$L = \frac{1}{2}\rho V^2 S C_L \tag{18}$$

$$M = \frac{1}{2}\rho V^2 S l C_m - \frac{3}{2}\frac{g}{r}(I_x - I_z)\sin(2\theta) \tag{19}$$

$$C_D = C_{D_0} + C_{D\alpha}\,\alpha^2 \tag{20}$$

$$C_L = C_{L0} + C_{L\alpha}\,\alpha \tag{21}$$

$$C_m = C_{m0} + C_{m\alpha}\,\alpha + C_{mq}(q - \dot{\mu}) + C_{m\delta bf}\,\delta bf \tag{22}$$

where:

ρ	=	atmospheric density (slug/ft^3)
C_D	=	nondimensional drag coefficient
C_{D0}	=	basic drag coefficient
$C_{D\alpha}$	=	partial derivative of C_D w.r.t. alpha (1/rad)
C_L	=	nondimensional lift coefficient
C_{L0}	=	basic lift coefficient
$C_{L\alpha}$	=	partial derivative of C_L w.r.t. alpha (1/rad)
C_m	=	nondimensional aerodynamic moment coefficient
C_{mq}	=	partial derivative of C_m w.r.t. pitch rate (sec/rad)
$C_{m\alpha}$	=	partial derivative of C_m w.r.t. alpha (1/rad)
$C_{m\delta bf}$	=	partial derivative of C_m w.r.t. body flap deflection (1/deg)
g(r)	=	gravitational acceleration (ft/sec^2)
l	=	characteristic length (vehicle length) (ft)
S	=	area of lifting surface (ft^2)

The final term in eqn(22) represents the contribution of the body flap deflection to the moment coefficient and is used as a standard pitch control surface. The density is calculated using one of two analytic expressions depending on the altitude. The specifics of how the density is calculated as well as a brief discussion of the development of the analytic expressions is found in Appendix 2.

Thrust Laws. Three basic ideal thrust laws are used in this study. The equations representing these thrust laws are detailed below.

constant thrust rocket

$$T = \frac{1}{2}\rho_0 V_0^2 S C_{D0} \tag{23}$$

where: ρ_0 = atmospheric density at starting altitude (slug/ft^3)
V_0 = velocity at starting altitude (ft/sec)
C_{D0} = drag coefficient at starting altitude

Notice for the constant thrust case the thrust is fixed at the values of the drag for the starting altitude (i.e. the altitude where the bifurcation sweeps starts). This is required since to start the continuation method an equilibrium solution must be provided as a first step. In all cases the equilibrium solution has $\alpha = \theta = 0$ radians. This requires the thrust to equal the drag for equilibrium.

variable thrust rocket (6:356)

$$T = \dot{m} V_{exh} + (P_e - P_a) A_n \tag{24}$$

As stated above the starting equilibrium point with $\alpha = \theta = 0$ radians requires the thrust to equal drag when the continuation method is begun. This requires that the mass flow be determined by setting the thrust equal to the drag at the starting altitude, therefore the mass flow rate of the exhaust is fixed at the following equation. Note it is assumed the mass flow is sufficiently small relative to the mass of the vehicle as to be negligible. This assumption is fairly good at high altitude but is very

poor at altitudes below about 200,000 ft.

$$\dot{m} = \frac{\frac{1}{2}\rho_0 V_0^2 S C_{D0} - (P_e - P_a) A_n}{V_{exh}} \tag{25}$$

where:
- A_n = exhaust nozzle area (ft^2)
- $\dot{m}$ = mass flow rate of exhaust (slug/sec)
- P_e = pressure at exhaust nozzle exit plane (psf)
- P_a = ambient air pressure (psf)
- V_{exh} = velocity of exhausted mass (ft/sec)

ideal turbojet (9:332)

$$T = T_0 \left(\frac{\rho}{\rho_0} \right)^x \tag{26}$$

As with the constant thrust rocket, thrust for the ideal turbojet must equal drag at the starting altitude since the continuation method requires an initial "starting" equilibrium solution and $\alpha = \theta = 0$ was taken as the values of these states at the equilibrium point. Therefore the value of T_0 is set by the following relation:

$$T_0 = \frac{1}{2}\rho_0 V_0^2 S C_{D0} \tag{27}$$

Note the exponent "x" can be used to change the way the thrust varies with altitude. For the standard turbojet, x equals one (x=1).

It should be noted that in all cases the thrust can be varied with in the subroutine CONST through a Thrust Scaling Parameter (δT) that multiplies the calculated value of thrust using the above relations.

This parameter thereby acts as a throttle, increasing or decreasing the thrust as required for the δT bifurcation sweeps.

Vehicle Characteristics. As with the majority of previous studies conducted on this subject, the vehicle geometry and aerodynamic characteristics used here will be basically the same as those used by Etkin (4:783-784). This allows nearly direct comparison of results which is helpful to check consistency of linearization at starting points and more importantly will be used to highlight the advantages and simplicity of using bifurcation analysis for even the simplest problems in atmospheric flight mechanics/dynamics. Etkin obtained his data from "*simple Newtonian impact theory for a slender body (cone or wedge of about 3° semiangle) at moderate angle* (4:784)." In this study a small change has been made to allow for lift at zero angle of attack, which is more representative of a hypersonic vehicle, however as seen in Figure 3 Etkin's basic lift to drag ratio was followed fairly well.

With these clarifications stated the geometry and aerodynamic characteristics are as follows:

Geometry

$l = 50$ ft $k_y = (I_y/m)^{1/2} = 25$ ft $k_0 = (I_x - I_z)/I_y = -0.94$
$W = 700{,}000$ lb $W/S = 30$ psf (at sea level)

Aerodynamics (dimensions are [rad^{-1}] unless otherwise indicated)

$C_{L0} = 0.05$
$C_{L\alpha} = 0.50$
$C_{D0} = 0.0133$
$C_{D\alpha} = 0.400$

$C_{m0} = 0.00$
$C_{m\alpha} = -0.0548$
$C_{mq} = -0.028$
$C_{m\delta bf} = -0.0822$ [deg^{-1}]

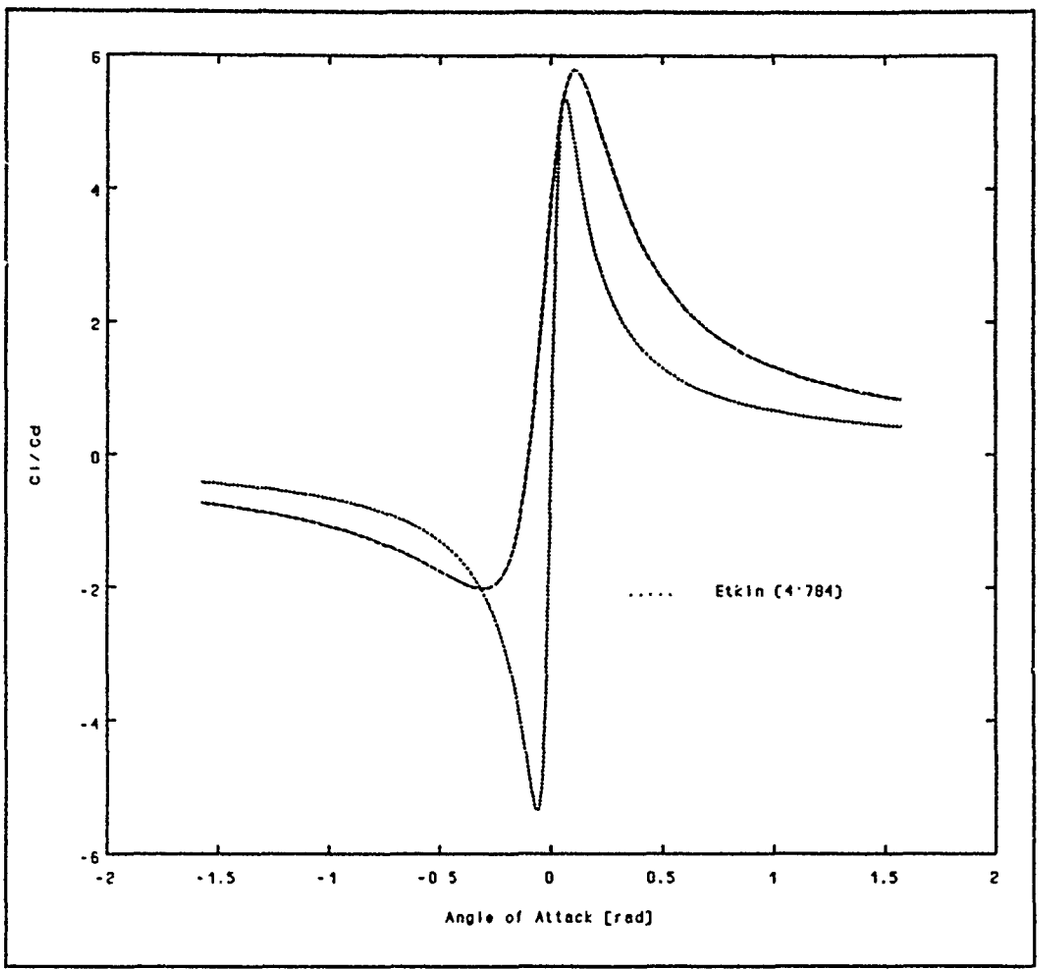

Figure 3. Comparison of C_L/C_D with Etkin's work

II. Introduction to Bifurcation Analysis and Stability

Equilibrium Solutions and Equilibrium Points

At this point it is best to discuss some of the central points of bifurcation analysis to allow the uninitiated to understand what is being done, and to highlight what is being presented in the bifurcation diagrams and phase plane diagrams which follow.

Continuation is the core on which the present application of bifurcation analysis is based. There are several types of continuation techniques, but discussing them is not appropriate here. What is required is a general description of what is obtained. The analysis here starts at an equilibrium point from which the continuation technique is begun. The equilibrium point is obtained by setting the time derivatives of the state variables to zero thus creating a set of homogeneous equations and solving simultaneously for the values of the state variables that satisfy the homogeneous equations. Once this starting point is obtained the continuation method can begin. The continuation method will search in the vicinity of this point until it finds another point which satisfies the set of homogeneous equations. This process continues over the given range of the specified parameter and within the bounds established for the states, until a complete parameter-dependent family of equilibrium solutions to the set of homogeneous equations has been found. An important feature of the bifurcation software AUTO is the ability to find the equilibrium solution path despite running into singular points (limit points and bifurcation points). AUTO uses a pseudo-arclength technique

which allows it to continue working despite encountering a singular Jacobian of the linearized set of equations. Other less robust techniques fail at these points where the slope of the solution with respect to the parameter is not unique, as in the case of a bifurcation, or undefined, as with a limit point. The reader is referred to the user's manual for AUTO and the text by Seydel for further information on this technique (3:12-16; 12:116+).

Simple Nonlinear Behavior:

While knowing an equilibrium solution branch is interesting, the true value in this analysis for those interested in nonlinear effects is the accurate location of limit and bifurcation points. The reasons for interest in these singular points are many. In the case of a bifurcation this point represents the intersection of other solution branch(es). Depending on the type of bifurcating point there is the potential for complex motion arising from the nonlinear nature of the problem. In the analysis of longitudinal motion of a powered lifting hypersonic vehicle the two most prevalent singular points encountered are limit points, which may give rise to hysteresis type behavior or an exchange of stability, and Hopf bifurcations, which generally occur in this study when the phugoid mode eigenvalues cross the imaginary axis transversely and either lose or gain stability. Generally for the analysis of the longitudinal dynamics of a powered lifting hypersonic vehicle the Hopf point signals the loss of stability in the phugoid mode. A Hopf point is of special interest in the study of nonlinear dynamics as the behavior subsequent to a Hopf bifurcation is generally characterized by increasingly complex periodic

motion known as limit cycles. For systems with three or more degrees of freedom the Hopf bifurcation may also be the first step in the direction of chaos (12:25).

While the mathematics of bifurcation analysis is not within the scope of this thesis an understanding of physical processes is. To further clarify some of the points made, and to provide a basis for understanding what a basic bifurcation study is all about, the following simple example is presented (10).

Figure 4 shows a mass (m) connected by a mass-less rigid rod to a mass-less rigid sleeve which is around a spinning shaft. The friction coefficient between the spinning rod and the sleeve is constant therefore a constant torque is generated which is transmitted to the mass as a force (F) via the mass-less rigid rod. In-set in Figure 4 is the free-body diagram for the mass and the reference axes. Note the pendulum is held at a constant angular position by the torque applied to the sleeve.

The scalar equation of motion for the mass m is:

$$mr\ddot{\theta} = F - mg\sin(\theta) \tag{28}$$

Where:
- F = force generated by the constant torque (F=T/r) [lb]
- g = gravitational acceleration (ft/sec^2)
- m = mass (slugs)
- r = length of rod (ft)
- T = torque applied to sleeve (ft-lb)

At a point of equilibrium the left hand side of eqn (28) is equal to zero, that is there is no change of the state variable when the forces acting on the mass are in equilibrium.

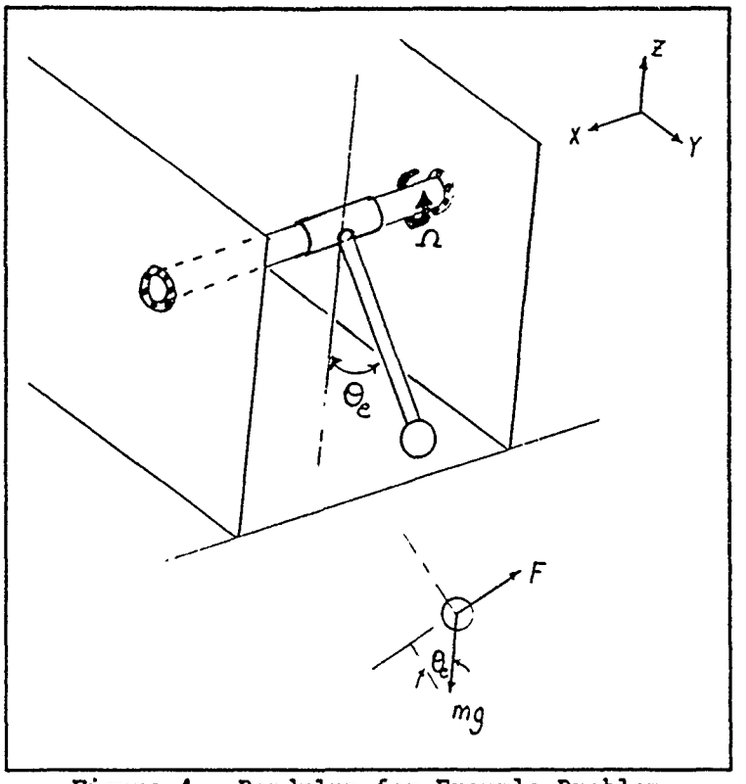

Figure 4. Pendulum for Example Problem

This brings out an important point to remember when looking at bifurcation diagrams: *the stationary solution path is made up of equilibrium solutions (equilibrium points) and no change of the state variables is involved.*

For the equilibrium solutions eqn (28) is a homogeneous equation. In the case of the powered lifting hypersonic vehicle there is a set of homogeneous equations that are solved to locate the equilibrium solution. To actually conduct the bifurcation analysis a parameter must be established for which the continuation process finds a solution path. For the example problem, the parameter can be identified as $\lambda = F/(mg)$ and

the homogeneous equation can then be put in the form of eqn(29) below:

$$\theta_e = \sin^{-1}\left(\frac{F}{mg}\right) \tag{29}$$

By varying λ from -1 to 1, a plot of the equilibrium solutions for θ_e is easily obtained even with a hand calculator. The bifurcation analysis however, yields information on stability by linearizing the differential equation (or set of equations) and solving for the eigenvalues of the subsequent Jacobian thus providing the following bifurcation diagram.

In looking at the bifurcation diagram it is seen there are at least two equilibrium solutions for each λ in the open set (-1,1). The two points corresponding to λ=-1 or 1 are called limit points. It is clear to see that limit points have only one value of the equilibrium point for a given parameter and are points where the equilibrium solution path turns back with respect to the parameter; thus the slope is undefined. Note also that to one side of a limit point no equilibrium solutions exist yet on the other side two equilibrium solutions exist for each λ. In the example problem the limit points also correspond to points where stability is either lost or gained, depending on the direction of the parameter λ, however this is not always the case for limit points in general. Finally, note the convention used in bifurcation diagrams is to identify stable equilibrium branches with solid lines and unstable equilibrium branches with broken or dashed lines; other graphical conventions will be brought to the reader's attention as required.

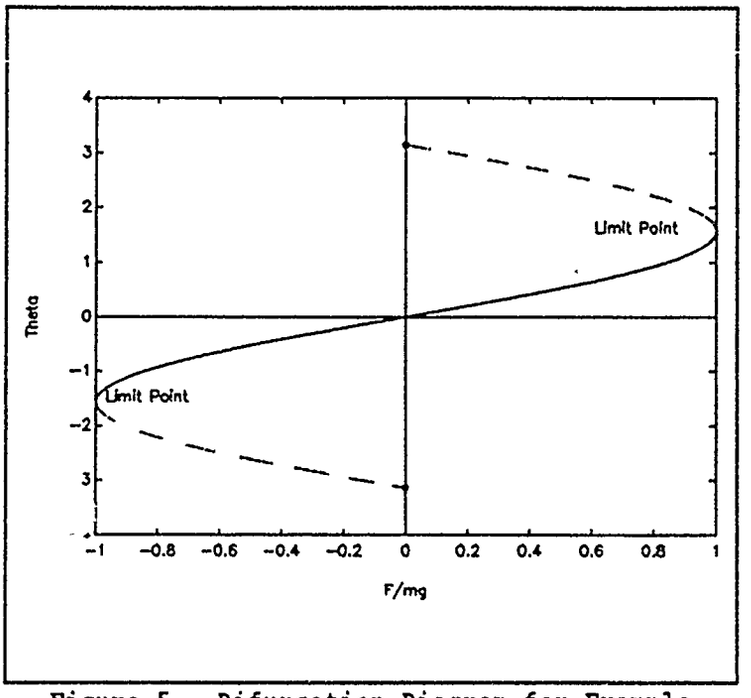

Figure 5. Bifurcation Diagram for Example Problem

The bifurcation diagram now shows part of its value in that the local, and at times global, behavior of trajectories can be predicted. For this example problem trajectories in the vicinity (domain of attraction) of a point on the stable equilibrium branches will oscillate about the equilibrium point since no damping is included. If damping were added the trajectories would be attracted to the equilibrium point. This can be visualized in thinking of the mass at an angle θ_e that corresponds with the stable branch for a given value of λ. Given a small perturbation in any direction the mass will return to the equilibrium point, that is it will be attracted to the stable branch. Trajectories in the vicinity (domain of repulsion) of a point on one of the unstable solution branches will be repelled. Again think of the pendulum mass at an angle θ_e that corresponds to a point on one of the unstable branches. Given a small

perturbation the mass will not return to its original position or trajectory but will move away and in the example problem will swing around the shaft. Note finally, that the domain of attraction can be limited. In the example problem, even if the mass is in a stable position in the lower part of the pendulums arc, if given sufficient perturbation in the direction of the force F the mass can be made to swing around the shaft and in the absence of any damping action will not settle back to a stable position; i.e. the domain of attraction is limited. Finally, note for values of $\lambda > 1$ and $\lambda < -1$ the pendulum will swing continuously about the shaft - - no equilibrium exists.

The foregoing example has provided a good picture of the very basics of bifurcations analysis and some of the phenomena that may occur when analyzing nonlinear problems. In addition it has provided some physical significance to limit points. It was however limited in its ability to fully demonstrate possible behavior as it has only one degree of freedom. Problems with three or more degrees of freedom can develop many other phenomena and a variety of ways to exchange stability.

Limit Cycles (Orbits)

Hopf bifurcations, which are a central feature in the study at hand, give rise to periodic solution branches which on a bifurcation diagram are shown by plotting the maximum and/or minimum values of limit cycles (Figure 6). These surfaces projected in the phase plane, or phase space for systems with degrees of freedom greater than two, are called limit cycles or orbits and represent a surface of periodic solutions surrounding a equilibrium solution branch (Figure 7).

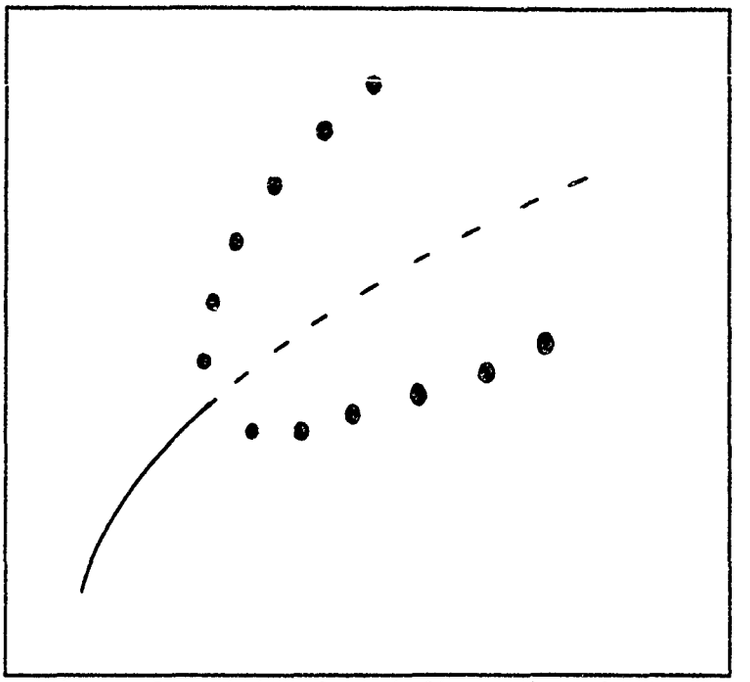

Figure 6. Limit of Periodic Motion about a Solution Branch

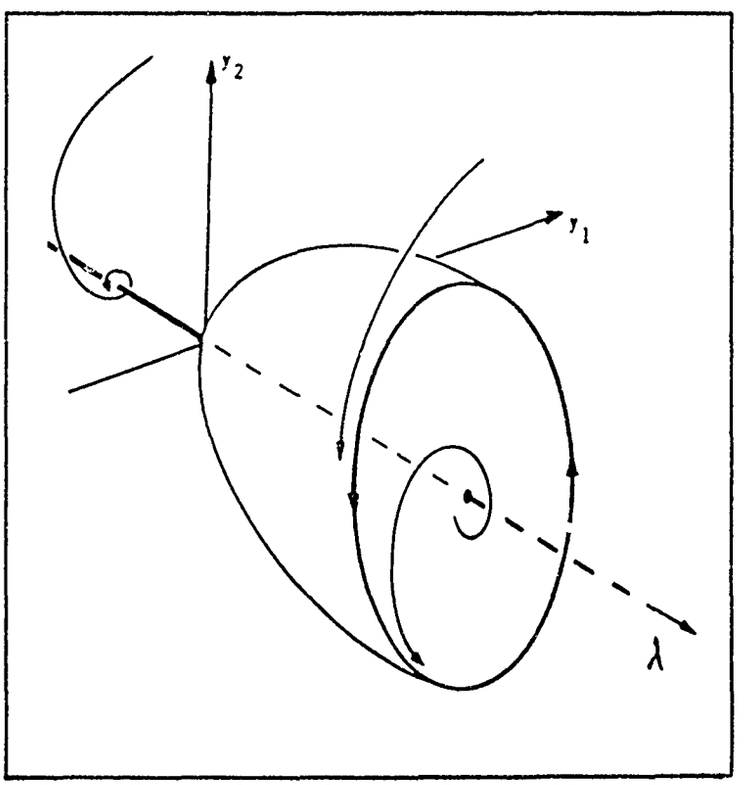

Figure 7. Limit Cycle or Orbit in Phase Space (12:63)

Just as with equilibrium solution branches, periodic solution branches can be stable or unstable and will either attract or repel trajectories within their domain of influence (12:12-25). Local stability of the periodic solutions is based on Floquet theory involving the monodromy matrix (12:240-248). For the purpose of this study one need only know the relationship of the eigenvalues of the monodromy matrix with the criteria for local stability of the periodic solution branch. The monodromy matrix always has one eigenvalue (Floquet multiplier) in the complex plane at z=1. This is subsequently used as a test for accuracy in calculating the other multipliers in AUTO. Through establishing a relationship between the remaining Floquet multipliers and a Poincaré map or return map it is determined that if the modulus of the remaining Floquet multipliers are each less than unity then the periodic solution is stable (i.e. attracting). AUTO computes the Floquet multipliers and uses this to determine stability. As mentioned above the accuracy of this calculation must be checked based on the one Floquet multiplier at z=1. Since five ordinary differential equations make up the full set of equations needed to model the longitudinal dynamics for this study then for the periodic branches to be stable four Floquet multipliers must each have a modulus less than unity and one must have a modulus equal to unity. Further discussion of nonlinear behavior is beyond that required to begin the analysis, these concepts will be expanded on as the results of the study are examined.

Two Parameter Continuation:

Upon locating a Hopf bifurcation point or limit point AUTO can be used to perform a two parameter continuation which will show the evolution of bifurcation points as the second parameter is varied; ordinary equilibria is ignored. For the study here the two parameter continuation will be used to determine the value of a gain in a feedback loop to attempt to stabilize a system. Specifically by plotting one parameter against another a curve of limit points or Hopf points is generated. If for instance, the first parameter is the body flap deflection or a pitch command and the second parameter is the pitch rate feedback gain in a pitch attitude feedback loop, the plot of the two parameters would show how the Hopf point (the point of stability exchange) moves with the pitch rate gain. A typical plot might look something like Figure 8.
In this figure one can see that for values of pitch rate gain the Hopf point will move along the curve. If one wishes to delay the occurrence of the Hopf point relative to the magnitude of the body flap deflection (thereby delaying the exchange of stability) one would raise or lower the gain as appropriate until the Hopf point is moved far enough to meet the system requirements based on the body flap deflection. Some simple feedback techniques are examined further in Section IV.

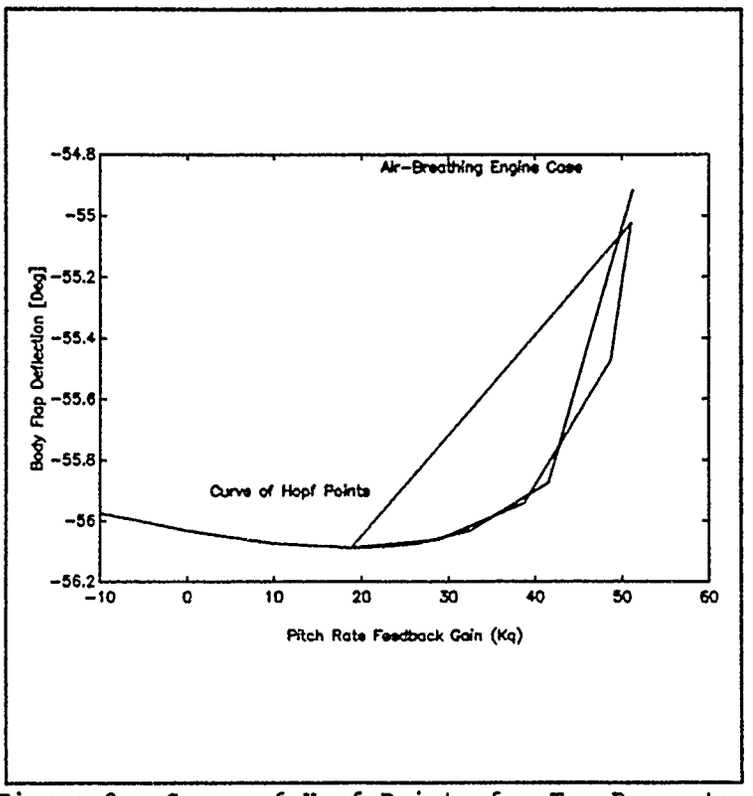

Figure 8. Curve of Hopf Points for Two Parameter Continuation with Pitch Rate Gain and Body Flap Deflection

III. Bifurcation Analysis of Longitudinal Dynamics

To begin the actual analysis the set of ordinary differential equations given by eqns(7,9,10,13 and 16) must be solved for an equilibrium point. As stated before this equilibrium starting solution is required for the continuation method to begin. Taking the equations of motion and substituting the force and moment coefficients yields:

$$\dot{V} = \frac{T}{m}\cos(\alpha) - \frac{\rho V^2 S C_D}{2m} - g\sin(\gamma) \tag{30}$$

$$\dot{\alpha} = q - \frac{T}{mV}\sin(\alpha) - \frac{\rho S V C_L}{2m} + \frac{g(r)}{r}\cos(\gamma) \tag{31}$$

$$\dot{\theta} = q + \frac{V}{r}\cos(\gamma) \tag{32}$$

$$\dot{q} = \frac{\rho V^2 S l C_m}{2I_y} - \frac{3}{2}\frac{g}{r}\left(\frac{I_x - I_z}{I_y}\right)\sin(2\theta) \tag{33}$$

$$\dot{r} = V\sin(\gamma) \tag{7}$$

where the force and moment coefficients are as defined before in eqns(20, 21 and 22) and are again repeated below for convenience.

$$C_D = C_{D_0} + C_{D\alpha}\,\alpha^2 \tag{20}$$

$$C_L = C_{L0} + C_{L\alpha}\,\alpha \tag{21}$$

$$C_m = C_{m0} + C_{m\alpha}\,\alpha + C_{mq}\,(q - \dot{\mu}) + C_{m\delta bf}\,\delta bf \qquad (22)$$

The equilibrium values are obtained by first setting the left hand side of equations (7, 30, 31, 32 and 33) to zero and solving for the states (V, α, q, θ, and r). To make things easy γ is set to zero ($\gamma = 0$), which means $\alpha = \theta = 0$. From this point the following equations are obtained that describe the requirements for equilibrium with $r = r_0$, $\alpha = \theta = 0$:

$$\gamma_0 = 0.0 \qquad (34)$$

$$V_0 = \left[\frac{g(r_0)\,r_0}{1+\left(\frac{\rho(r_0)\,S r_0 C_L}{2m}\right)}\right]^{\frac{1}{2}} \qquad (35)$$

$$q_0 = -\frac{V_0}{r_0} \qquad (36)$$

$$T(r_0) = \frac{1}{2}\rho(r_0)\,SC_D V_0^2 \qquad (37)$$

$$C_m = 0.0 \qquad (38)$$

This set of equations is programmed into the user provided subroutine FUNC which AUTO requires to find the flow of equilibrium solutions as a specified parameter is varied. Note the body flap parameter (δbf) shows up in the last term of eqn(22). Also of interest is the value of the thrust at the starting equilibrium point - - it equals the drag as was discussed earlier for the thrust laws. The AUTO software package was used to develop the equilibrium solution branches and identify bifurcation

points for the system described by eqns(7, 30, 31, 32 and 33). The parameters used to conduct the analysis were a body flap parameter (δbf) and a parameter which scaled the thrust (δT); simulating a throttle. This study was conducted for several starting equilibrium altitudes, which amounts to selecting a starting altitude ($r = r_0$), and setting the angle of attack and pitch angle to zero and letting AUTO solve for the velocity, pitch rate and thrust. The starting altitudes ranged from 50,000 ft to 700,000 ft. Again note that for each starting equilibrium altitude a different value of the initial equilibrium thrust is obtained since, as discussed before, thrust must equal drag at the starting equilibrium point. Note that the thrust decreases with increasing altitude. The resulting bifurcation diagrams are identified by their starting altitude as the thrust level, which is fixed by the drag at the starting altitude, makes a difference in the behavior of the system.

One can see the equations of motion are clearly nonlinear with the states all interrelated, However two states exert the primary influence by virtue of the type of problem being analyzed, these are the velocity and the radius. It is the way these two states vary to achieve equilibrium and the fact that the behavior being observed is the behavior of the equilibrium solution path that makes for results that are not intuitively obvious relative to the effects of changing the body flap or throttle (or more precisely thrust variations). This point must be emphasized since most traditional dynamists are used to dealing with the time history of trajectories or frequency response given some control input. As discussed in section II the bifurcation diagrams which are used here are not time histories but a collection of equilibrium points that provide the value of the states relative to a parameter.

The fact that the solution branch is made up of equilibrium points implies that no change of the state variables occurs at the individual points along the curve; this can at times cause confusion so beware.

Three cases were initially considered based on the three separate thrust laws discussed in previous sections. The results of the rocket whose thrust varied with altitude differed little from the more standard constant thrust rocket used by most previous authors working on this topic so the case was dropped. The remaining two cases were studied to investigate the behavior the rather simple nonlinear model would generate. What follows is a discussion of the results. Since the effect of the body flap and throttle are significantly different it is best to discuss them separately.

Body Flap Parameter (δbf) Variation

The body flap parameter mathematically represents a deflection of the body flap in degrees. This value is changed to radians and affects the value of C_N via eqn(22). A change in the value of C_N generally causes a change in the vehicles angle of attack and pitch attitude. It is interesting to note that the primary influence of the body flap on the behavior of the equilibrium solution path is, that in changing the angle of attack the value of the lift coefficient is changed which is a key parameter in establishing the value of the velocity for a equilibrium orbit (16:321-344). Therefore it is best to think of the body flap as a control by which lift is modulated.

To understand the equilibrium solutions obtained relative to the body flap parameter one must examine the relationship of the velocity and

radius with C_L. The following equation relates the velocity to C_L and radius and is central in understanding what is occurring when looking at a equilibrium solution path displayed in a bifurcation diagram.

$$V^{*} = \sqrt{\frac{r\left(g - \frac{T\sin(\alpha)}{m}\right)}{1 + \frac{\rho S C_1 r}{2m}}} \tag{39}$$

This equation results from the homogenous set of equations for equilibrium and represents the velocity - altitude relationship for everything from an unpowered satellite or lifting vehicle in equilibrium orbit to the case here of a powered lifting vehicle in equilibrium orbit. The velocity plays a key role in providing forces sufficient to balance the weight of the vehicle. At high altitudes the centrifugal force is the primary means by which the vehicle balances the weight, where at lower altitudes the lift, which is a function of velocity is the primary balance to the weight. The way in which the equilibrium solution path moves in order to balance all forces is quite interesting and as stated before not always obvious. Those interested in knowing more about how velocity, altitude and the lift coefficient are related in orbital flight are refered to reference (16).

The investigation was conducted by performing a continuation from the equilibrium starting point (i.e. $r=r_0$) using the body flap parameter to control the initial direction of the continuation. A body flap sweep is defined as the summation of the equilibrium branches obtained from performing the continuation in the directions associated with a positive flap deflection and a negative flap deflection (control surface movement

downward being positive). The flap was constrained to +/- 90 degrees by fixing the limiting values for the parameter in AUTO. Starting altitudes for the constant thrust rocket case were varied between 100,000 ft and 700,000 ft and for the air-breathing engine case ranged from 50,000 ft to 400,000 ft. Note in all cases as the starting altitude is increased the starting equilibrium value of the thrust is decreased. The equilibrium solution paths were tabulated, stability determined and all simple bifurcations, limit points and Hopf bifurcation points were located. Having mapped out the equilibrium solution and identified the various singular or bifurcation points any Hopf bifurcations were continued to obtain the limit cycles. This process is accomplished by taking the equilibrium conditions at the point identified as a Hopf bifurcation as a starting point for AUTO's continuation method. Specific software routines in AUTO are used to perform the required functions to obtain the periodic solution branch. These data are generally interpreted graphically to obtain a general feel for the local behavior of trajectories in the vicinity of the solution branches; these graphs are known as bifurcation diagrams. Since bifurcation diagrams are meant to convey information about the behavior of the system, it seems only natural that a method or convention be established for presenting data on these. The reader is encouraged to take note of the following rules for conveying information about the types of solution branches and their local stability characteristics.

Equilibrium solution branches are presented as lines. Solid lines indicate stable solution branches and any type of broken or dashed lines indicate an unstable equilibrium solution branch.

Periodic solution branches are shown as circles or dots which

generally indicate the maximum amplitude of the periodic motion. Stable periodic solution branches are shown as solid dots or filled circles. Unstable periodic solution branches are indicated by open circles.

These conventions are adhered to throughout this paper.

Constant Thrust Rocket Case. The following bifurcation diagrams were generated using AUTO as described previously, however further explanation of the way the constant thrust value is determined. As stated several times before, and shown explicitly in eqn(37), the thrust equals the drag at the starting equilibrium solution with $\gamma = 0$ radians. For the constant thrust rocket case this value obviously is fixed over the entire body flap sweep. This means that two equilibrium solution points with the same altitude but obtained from body flap sweeps starting at two different altitudes will not have the same value of thrust and in general will have different values for the other states as well. Note finally, as starting altitudes are increased the value of the thrust decreases.

Figures 9 and 10 show a collection of bifurcation diagrams for each state (note $\alpha = \theta$) for the body flap (δ_{bf}) sweeps from 100,000 and 300,000 ft respectively. While the behavior is nonlinear there is not a great deal of interest occurring over most of the equilibrium branches. Figure 9 is characteristic of the constant thrust rocket case with δ_{bf} as the parameter for starting altitudes less than 150,000 ft and Figure 10 is characteristic of the constant thrust rocket case with δ_{bf} as the parameter for starting altitudes between 150,000 ft and about 360,000 ft. One of the first things to note in each figure is the system is unstable (indicated by the dashed line).

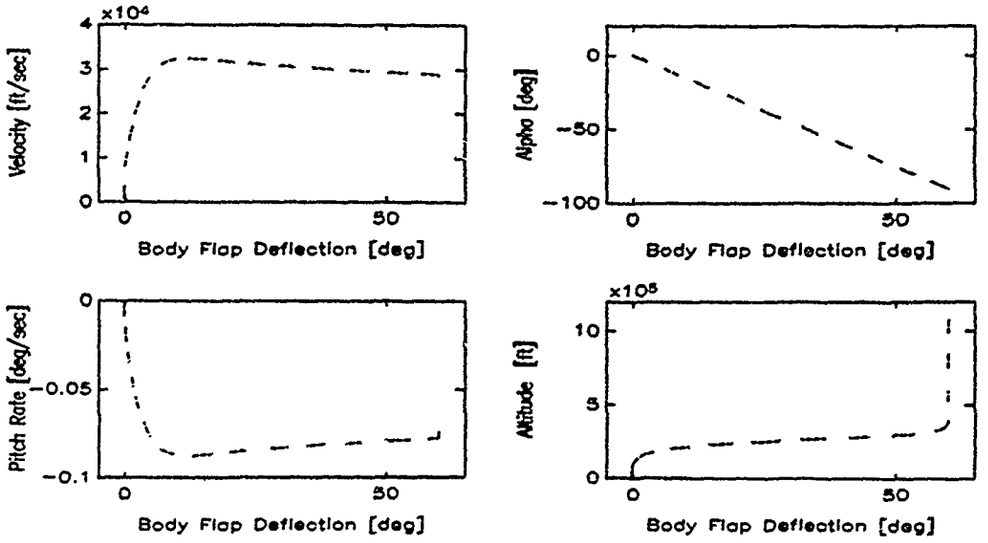

Figure 9. Bifurcation Diagrams for Body Flap Sweep from 100 kft Constant Thrust Rocket

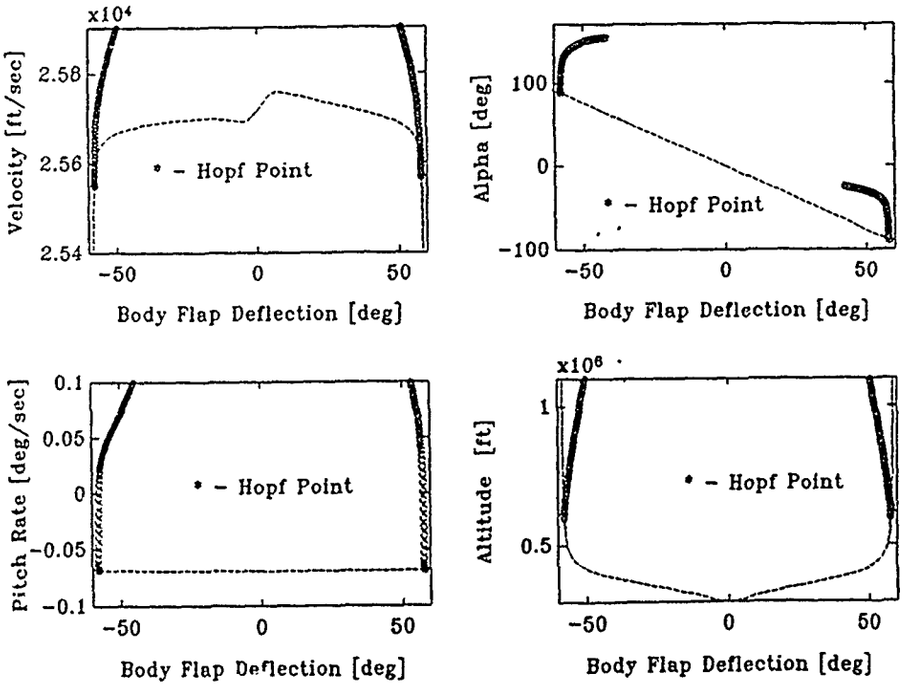

Figure 10. Bifurcation Diagrams for Body Flap Sweep from 300 kft Constant Thrust Rocket

The instability is caused by the nonoscillatory height mode and was the case for both thrust laws representing a rocket. This behavior is consistent with the previous studies and follows as a result of the way the sum of the longitudinal forces change with respect to altitude (13:472; 7:283). Interestingly enough the height mode would generally stabilize at some point for starting altitudes between about 360,000 ft and 530,000 ft and would occur associated with a limit point. Frustratingly this is about the point where the mode normally thought of as the phugoid mode (based on the longer period) would go unstable.

From the stand point of nonlinear analysis not much of interest is occurring for the body flap sweeps with starting altitudes less than about 360,000 ft. Specifically, the system is unstable with generally no limit points from which jump phenomena may occur and no simple bifurcations. Only if the continuation of a equilibrium branch associated with increasing altitude is allowed to go long enough, to where the aerodynamic pitch damping is lost due to the very low density at very high altitudes, will a Hopf point be found. For the body flap sweep from 300,000 ft (Figure 10) the Hopf point occurs at δ_{bf} = +/- 57.9° , and an altitude of 615,120 ft for the branch associated with a negative body flap deflection and 614,970 ft for the other branch; this symmetric behavior is not as closely followed at lower starting altitudes where the thrust levels and densities are greater.

Concentrating now on the unstable periodic branches found from the body flap sweep from 300,000 ft one can see from the bifurcation diagrams in Figure 10 that as the unstable periodic branch progresses the amplitude of the limit cycles become fairly substantial, however the period is on the order of 5000 seconds and since the periodic branch is unstable

trajectories would not approach it. Recall that the limit cycles of a periodic branch, indicated by circles, show the maximum and/or minimum amplitude of the p · odic motion. The stability of the periodic branches is interesting in that it is just barely unstable with a conjugate pair of Floquet multipliers just outside the unit circle. The height mode at the point where the phugoid mode goes unstable is very near the imaginary axis with a time constant on the order of 10^5 seconds; this is consistent with previous studies (4:786).

Figure 11 shows the time history over one period for the right periodic branch with δ_{bf} = 56.73° and δ_{bf}= 42.25°. Figure 12 shows the time history over one period for the left periodic branch with δ_{bf} = -56.6° and δ_{bf} = -41.8°. Note that near the Hopf point on either branch the motion is slight (ie just leaving equilibrium) but as the parameter is changed to move along the periodic branch the motion increases. Once again the behavior of the periodic branches shown in this body flap sweep (from 300,000 ft) is characteristic of the behavior of the periodic branches occurring from body flap sweeps starting at "lower" altitudes that subsequently extend to altitudes above 500,000 ft where pitch stability is lost.

In order to provide a complete look at the periodic behavior of the limit cycles, as well as provide a connection with more classic longitudinal analysis, the limit cycles are projected into the phase plane with the flight path angle. Figure 13 shows two limit cycles from the right periodic branch; one for δ_{bf} = 56.7° and one for δ_{bf} = 42.25°. Figure 14 shows two limit cycles from the left periodic branch; one at δ_{bf} = -56.64° and one for δ_{bf} = -41.8°. In looking at these figures one sees clearly that motion is associated with the periodic branches.

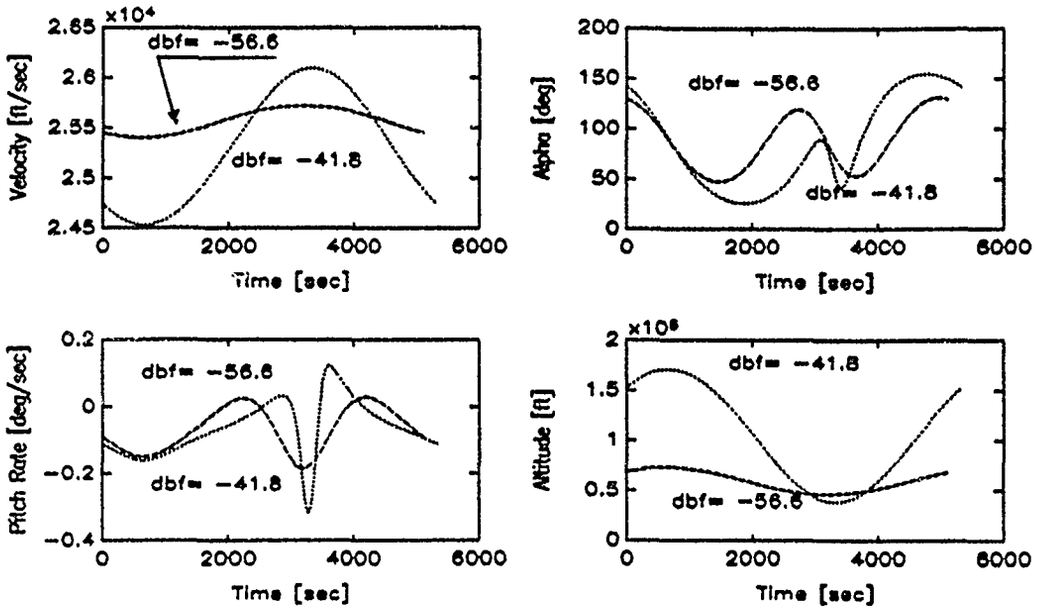

Figure 11. Left Branch Limit Cycles for δ_{bf} = -56.6° and -41.8° Body Flap Sweep from 300 kft : Const Thrust Rocket

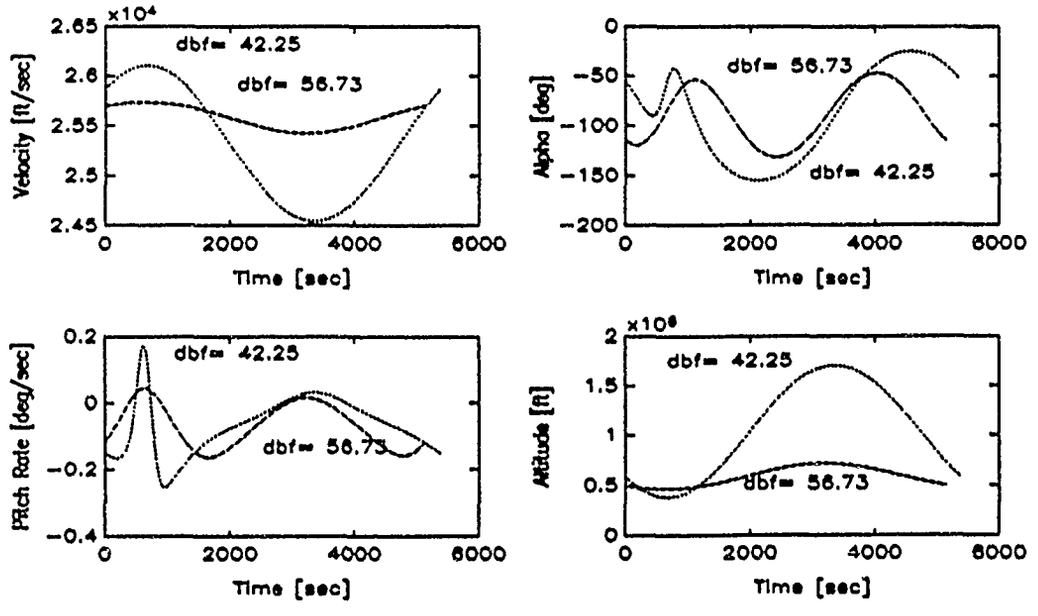

Figure 12. Right Branch Limit Cycles for δ_{bf} = 56.73° and 42.25° Body Flap Sweep for 300 Kft : Const Thrust Rocket

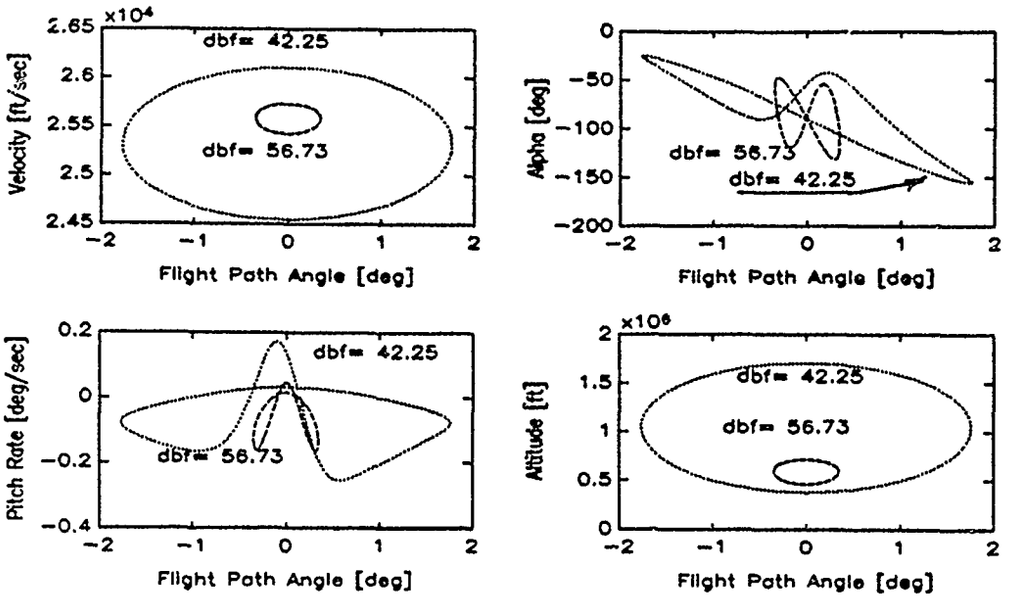

Figure 13. Right Branch Limit Cycles in Phase Plane for δ_{bf} = 56.73° and 42.25°. Sweep from 300 kft : Const Thrust Rocket

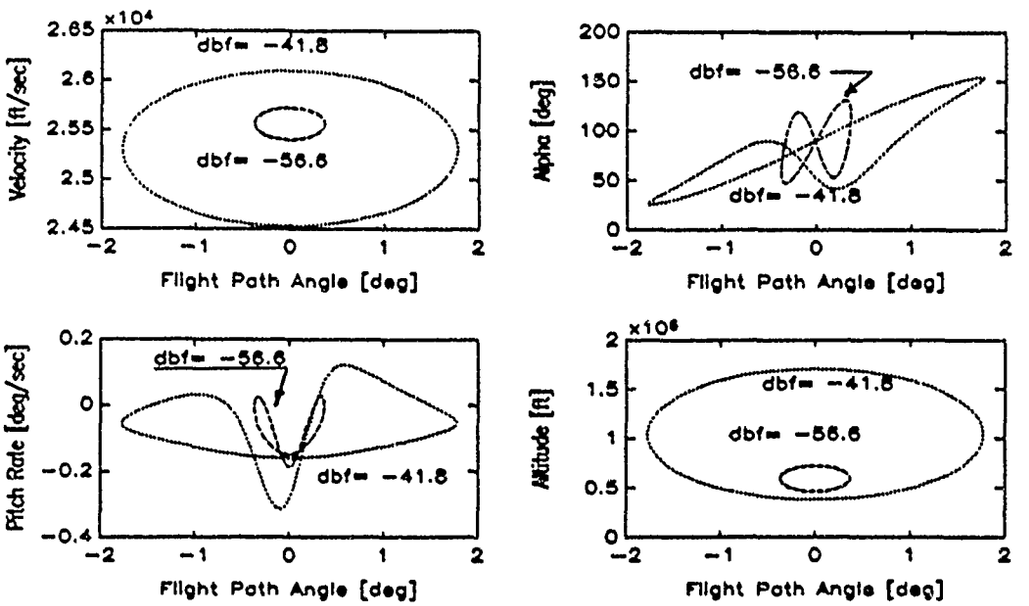

Figure 14. Left Branch Limit Cycles in Phase Plane for δ_{bf} = -56.64° and -41.8°. Sweep from 300 kft : Const Thrust Rocket

Also, the behavior of the translational states is very much like the classic phugoid mode, i.e. showing a steady exchange of potential and kinetic energy. While the periodic branches are unstable, the growth of the nonlinear behavior in velocity and altitude remains sinusoidal.In terms of the rotational states, one sees somewhat more complex behavior which should be expected since the periodic branches arose from the loss of pitch stability at the very high altitude.

The most interesting body flap sweep for the constant thrust rocket case resulted from the starting altitude of 400,000 ft. The body flap sweep bifurcation diagrams and expanded views for α and altitude are shown in Figures 15, 16 and 17. The behavior of the limit cycles of the periodic solution branches are certainly visually interesting. Note the periodic branches contain several limit points which explains their complex twisting about.

The Hopf bifurcation occurred at δ_{bf} = +/- 8.93° and generally speaking is not of great significance since the equilibrium branch was unstable to begin with and the periodic branch starts out unstable and encircles an unstable equilibrium branch. On closer inspection of the periodic branches one will see (Figures 16 and 17) that there is a portion of both periodic branches, starting at δ_{bf} = +/- 7.82° and continuing to δ_{bf} = +/- 6.05°, that gains stability by the crossing of a conjugate pair of Floquet multipliers. This type of stability exchange is associated with bifurcation to a torus. What this implies is that trajectories within the domain of attraction of the periodic branch will be drawn into periodic motion with two frequencies; one describing the component of the motion in the circumference direction of the torus and one around the cross section of the torus. The path of the trajectory can be visualized

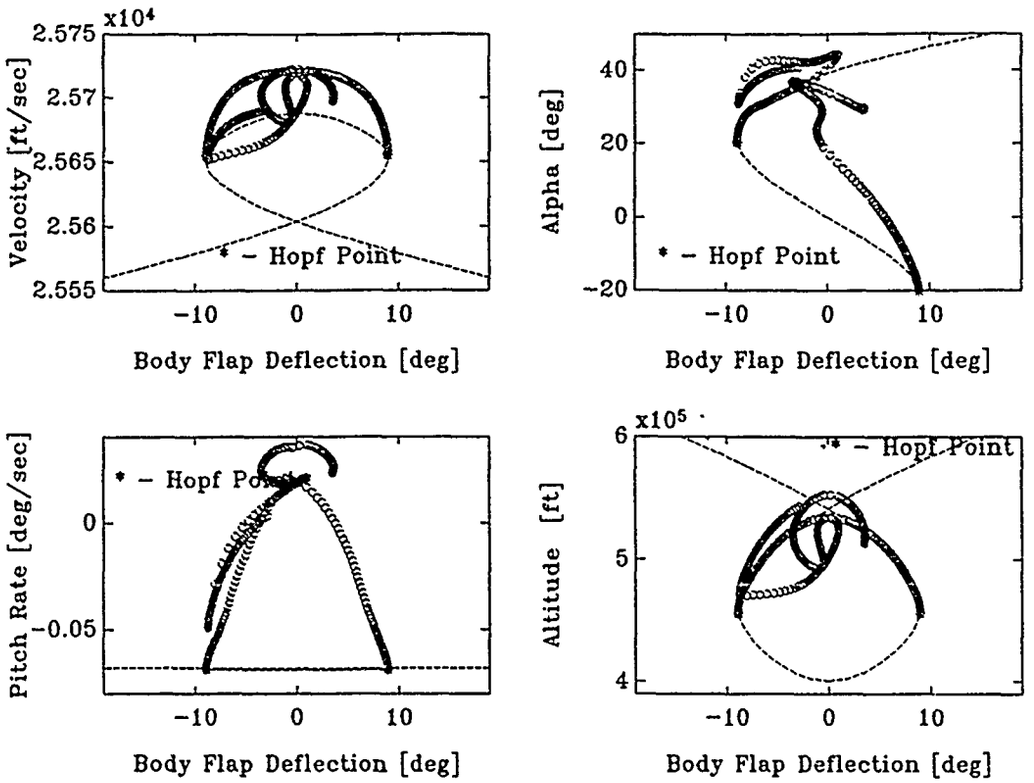

Figure 15. Bifurcation Diagrams for Body Flap Sweep from 400 kft Constant Thrust Rocket

as spiralling around the inside of an inner tube (i.e. torus) in hyperspace (12:263,264).

The accuracy of the solution is very good with the Floquet multiplier that is supposed to be equal to one (z=1), precisely equal to one. The fact that stability is gained then lost so quickly indicates that one or more Floquet multiplier(s) is(are) very near the edge of the unit circle and upon inspection of the output from AUTO one finds this to be the case with one pair inside the unit with modulus = 0.99884 and a second pair with modulus = 0.98. This would indicate a weakly attracting limit cycle for the range of δ_{bf} where the periodic branches are stable.

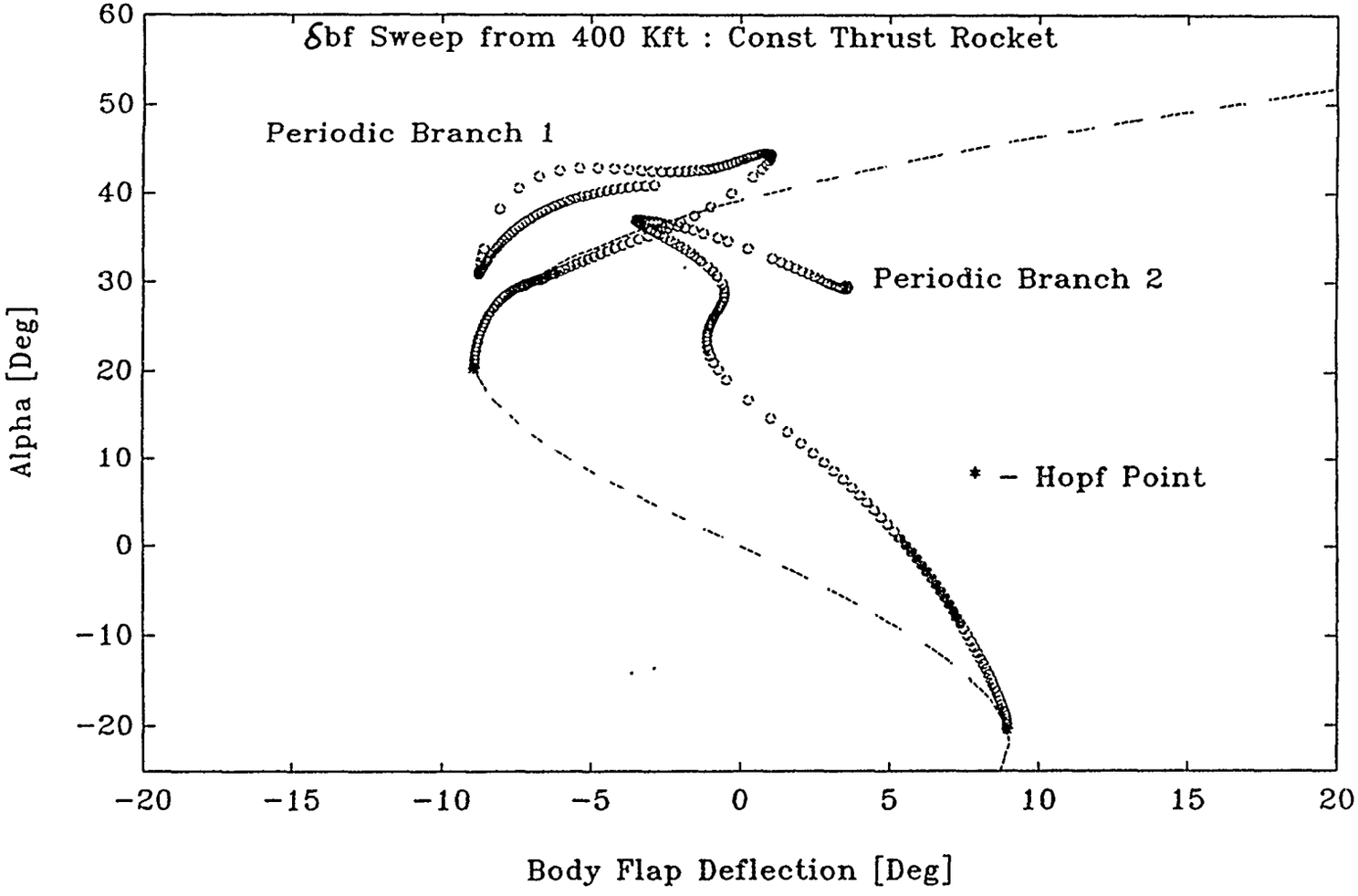

Figure 16. Bifurcation Diagram for Body Flap Sweep from 400 kft Constant Thrust Rocket

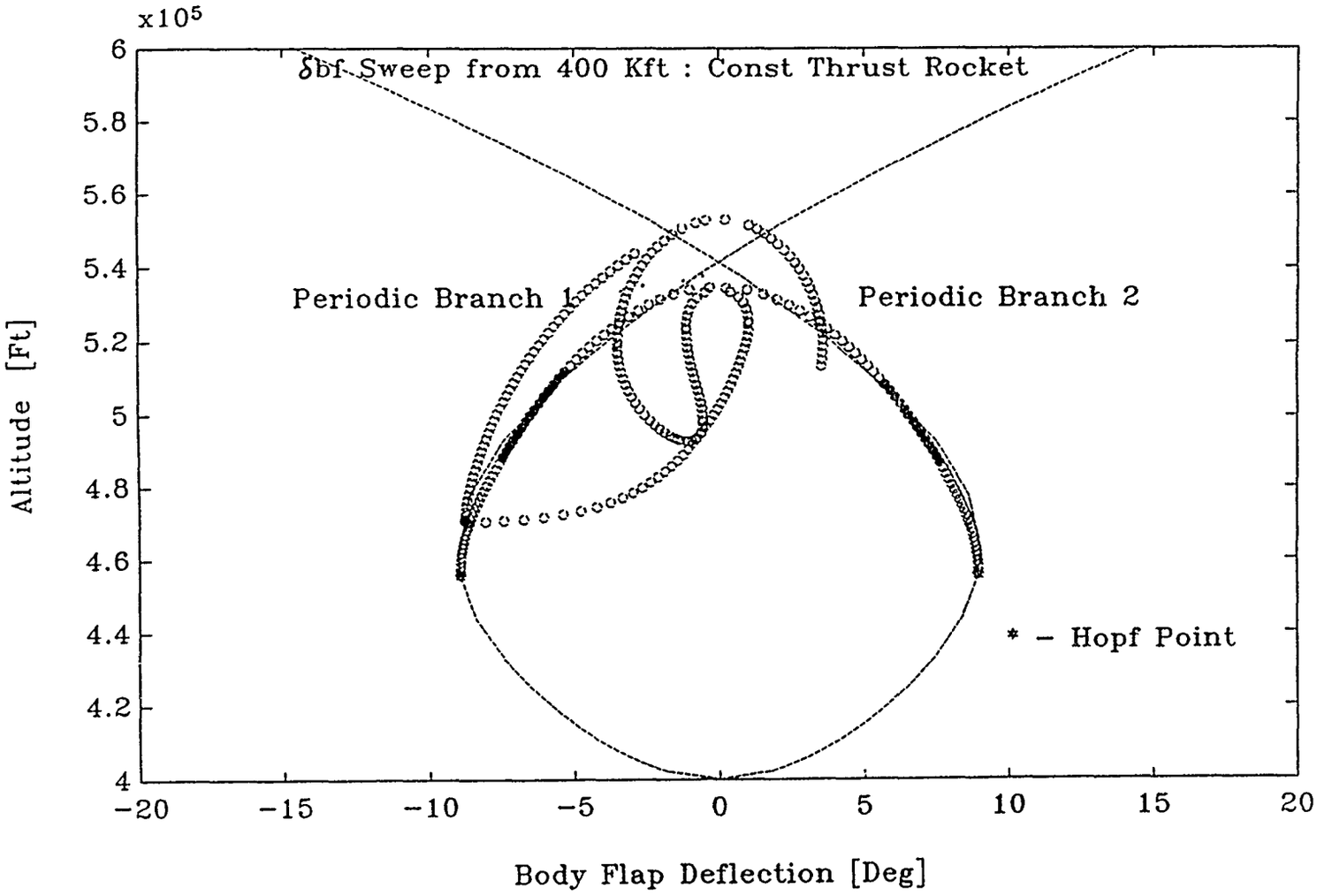

Figure 17. h Bifurcation Diagram for Body Flap Sweep from 400 kft Constant Thrust Rocket

Figure 18 shows the motion of the limit cycle over one period for periodic branch 1 (left branch) for a point in the stable region at $\delta_{bf} = -6.83°$ and a point near the end of the calculated portion of this periodic branch at $\delta_{bf} = -2.89°$. Figure 19 shows the motion of the same two limit cycles ($\delta_{bf} = -6.83°$ and $\delta_{bf} = -2.89°$) over one period in the phase plane with the flight path angle. Figure 20 shows the motion of the limit cycle over one period for periodic branch 2 (right branch) with $\delta_{bf} = 8.73°$ in the stable region and for $\delta_{bf} = 3.57°$ near the end of the calculated branch. Figure 21 shows the limit cycles at $\delta_{bf} = 8.73°$ and $\delta_{bf} = 3.57°$ in the phase plane with flight path angle. Observing the behavior of the limit cycle over one period at several points like this shows why the nonlinear behavior associated with period solutions are so interesting. Looking at Figures 18 and 20 one can see a kind of wave changing in amplitude as the parameter is varied. Figure 22 shows qualitatively the growth of the nonlinear behavior in α as periodic branch 2 grows. It is this type of behavior, for systems with three or more degrees of freedom, that leads to more fascinating subjects like chaos and the Hopf point is as Seydel puts it, "the door which opens from the small room of equilibria to the large hall of periodic solutions (12:61)."

On a somewhat different note, the altitude where the Hopf point occurs on both branches is just about 450,000 ft. This is in the altitude range where Etkin determined, and later others modified, that the period of phugoid and pitching modes came very close to each other (4:787-788; 15:17-20). The general conclusion of these earlier works is that there would be significant coupling of the two modes at this so called "resonance altitude" (15;7).

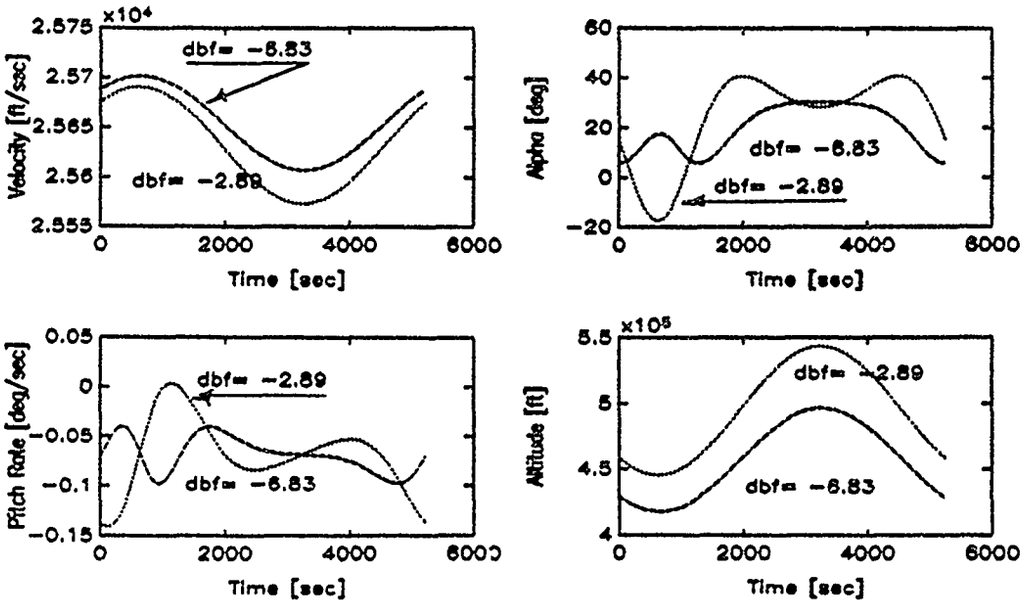

Figure 18. Limit Cycles for Periodic Branch 1 (δ_{bf} =-6.826° & -2.89°) Body Flap Sweep from 400 kft : Const Thrust Rocket

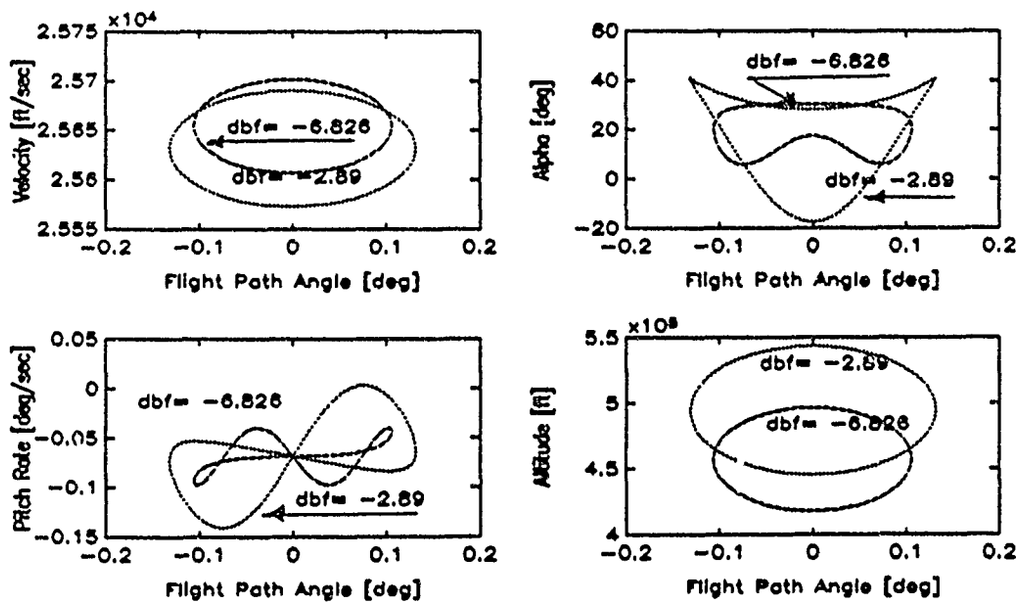

Figure 19. Limit Cycles in Phase Plane, Periodic Branch 1 (δ_{bf} = -6.826° & -2.89°) : Constant Thrust Rocket

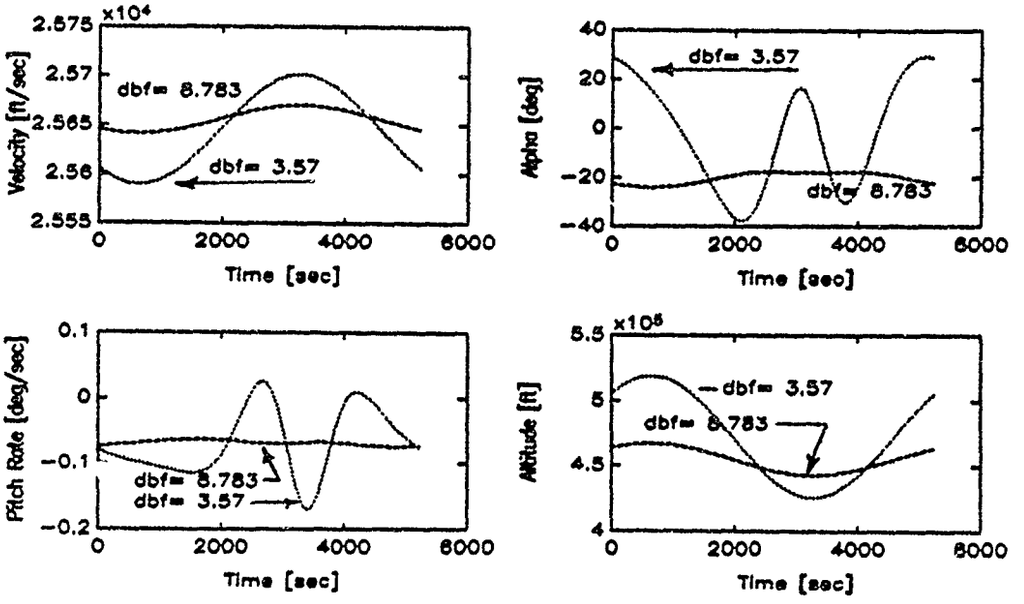

Figure 20. Limit Cycles, Periodic Branch 2, (δ_{bf} = 8.738° & 3.57°) Body Flap Sweep from 400 kft : Const Thrust Rocket

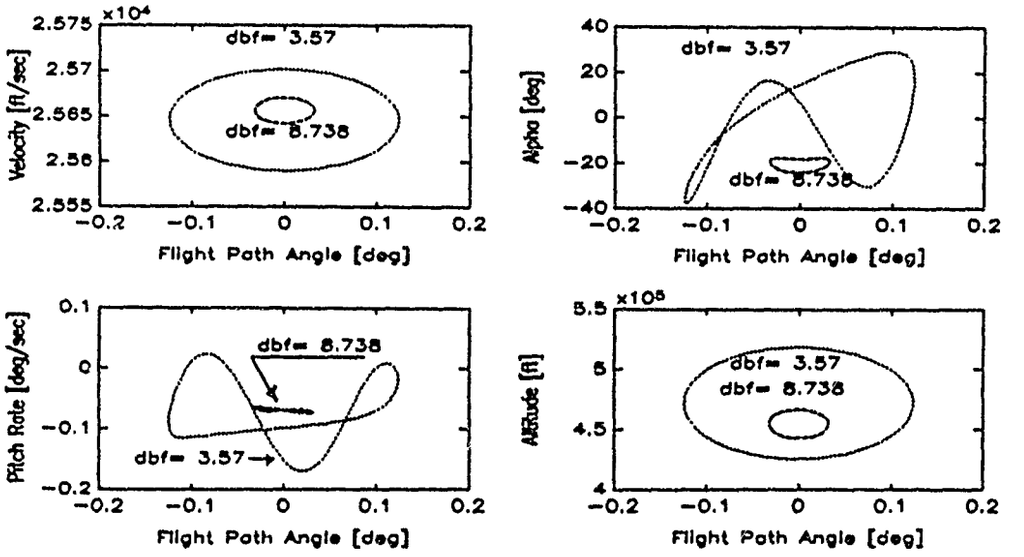

Figure 21. Limit Cycle in Phase Plane, Periodic Branch 2 (δ_{bf} = 8.738° & 3.57°), Sweep from 400 kft : Const Thrust Rocket

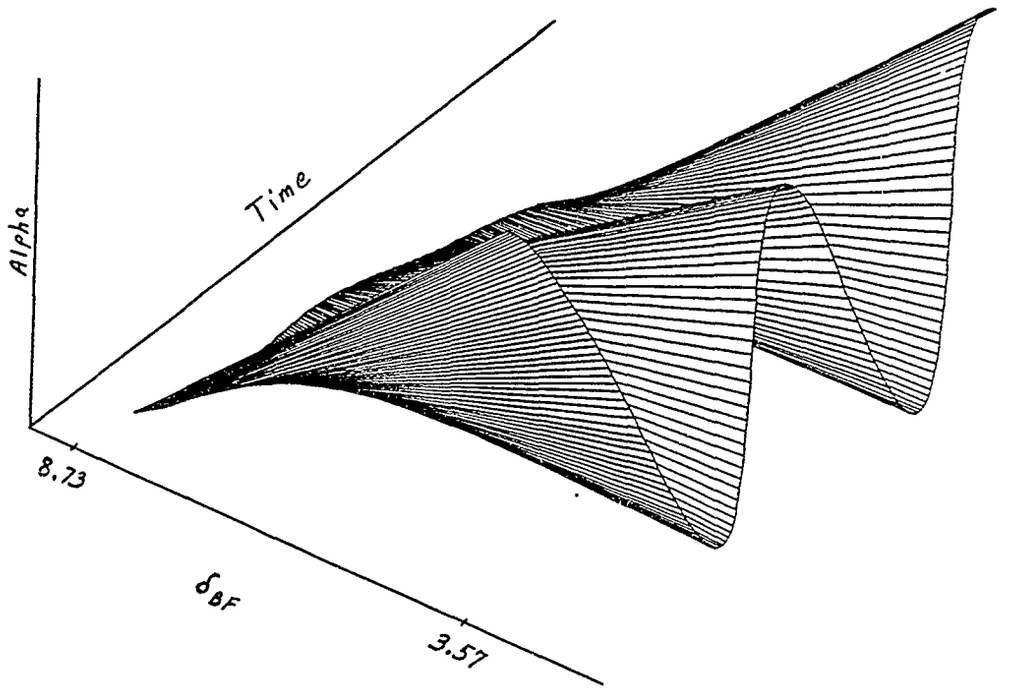

Figure 22. Growth of Nonlinear Waveform, Periodic Branch 2, α Bifurcation Diagram, Body Flap Sweep from 400 kft

In looking at the limit cycles in the preceding figures there does not seem to be the strong coupling predicted. Some coupled motion is evident in that the rotational states (α, θ, and q) go through sub-oscillations in each overall period while the translational states maintain a sinusoidal motion with a very regular period. Since the period is nearly that of the circular orbit for the same geocentric radius, it would seem that what is observed is a barely unstable elliptical orbit with the vehicle pitching about its y-axis at some sub-frequency greater than the frequency of the orbit (i.e. overall frequency of the limit cycle for the given parameter).

As a final note, notice the limit points on the equilibrium branch where the equilibrium solution path changes direction.

It is interesting in that it exists and is associated with the height mode stabilizing. Notice how the direction of the body flap deflection changes in order to maintain the original direction of the equilibrium solution path.

Air-breathing Engine Case. The procedure for continuation and subsequent analysis for the air-breathing case with the body flap as the parameter, was the same as that for the constant thrust rocket analysis. The results are somewhat more interesting in that the height mode is generally stable for the air-breathing case below approximately 380,000 ft thus the entire system is stable at these "lower" altitudes.

A phenomenon of little physical significance, but interesting nonetheless for the air-breathing case with body flap sweeps starting from equilibrium points between approximately 100,000 ft up to approximately 360,000 ft is that the velocity goes very nearly to zero for the portion of the body flap sweep that has a negative body flap deflection. Before the velocity actually gets to zero, a Hopf bifurcation occurs, then a simple bifurcation which has two solution branches. Of the two branches one stable and back-track the original equilibrium solution branch for all the states, and the other is unstable. The unstable branching solution back-tracks α, and altitude, but takes the negative of it's original value for velocity and pitch rate. Figure 23 shows this bifurcation diagram for the equilibrium branches only. Further work is needed to finish exploring this behavior. Notice that in Figure 23 the + - symbol indicates the stable branching solution and the x - symbol indicates the unstable

branching solution. Finally the original branch also turns back on itself after going to nearly zero subsequent to the Hopf point; this back-tracking original branch turns back as an unstable branch but regains stability as it repasses the Hopf point (as expected).

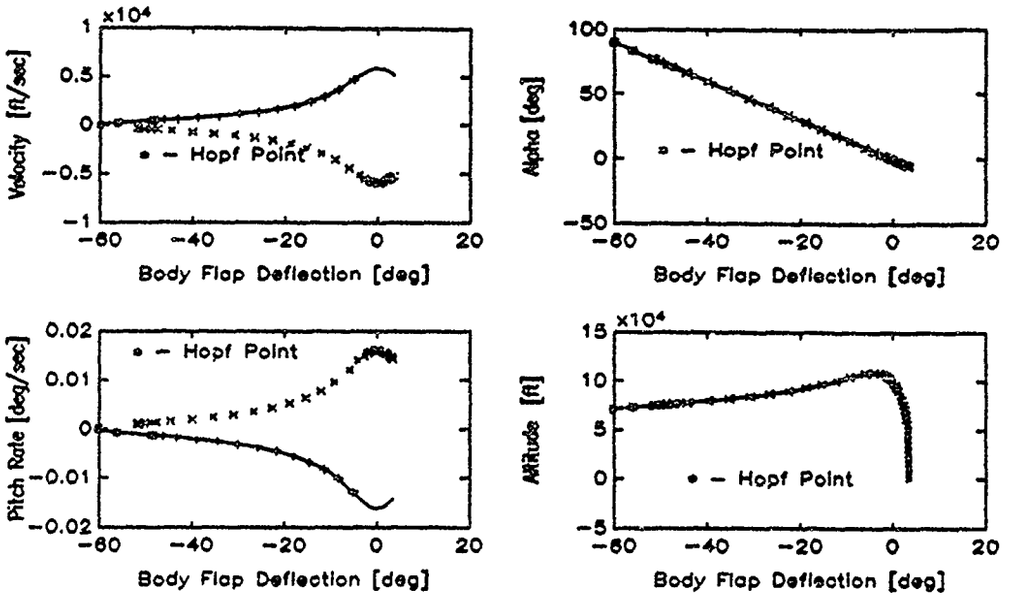

Figure 23. Bifurcation Diagram for Body Flap Sweep from 100 kft Air-Breathing Engine

For ease of discussion, Figure 24 shows all of the positive body flap sweep from 100,000 ft, but only the stable portion of the negative body flap sweep from 100,000 ft for the air-breathing engine case. This diagram contains the Hopf bifurcation but none of the "back-tracking" solutions. A big difference from the previous case is readily apparent, the system is stable up to the Hopf point at which time the phugoid mode loses stability and note how low the altitude is (approximately 73,000 ft). Notice this is a subcritical bifurcation (12:72); that is an unstable periodic branch encircles a stable equilibrium branch. What this

implies is trajectories near the periodic solution branch but within the domain of attraction of the equilibrium branch will be drawn to the stable equilibrium branch and generally no further changes of the states will occur.

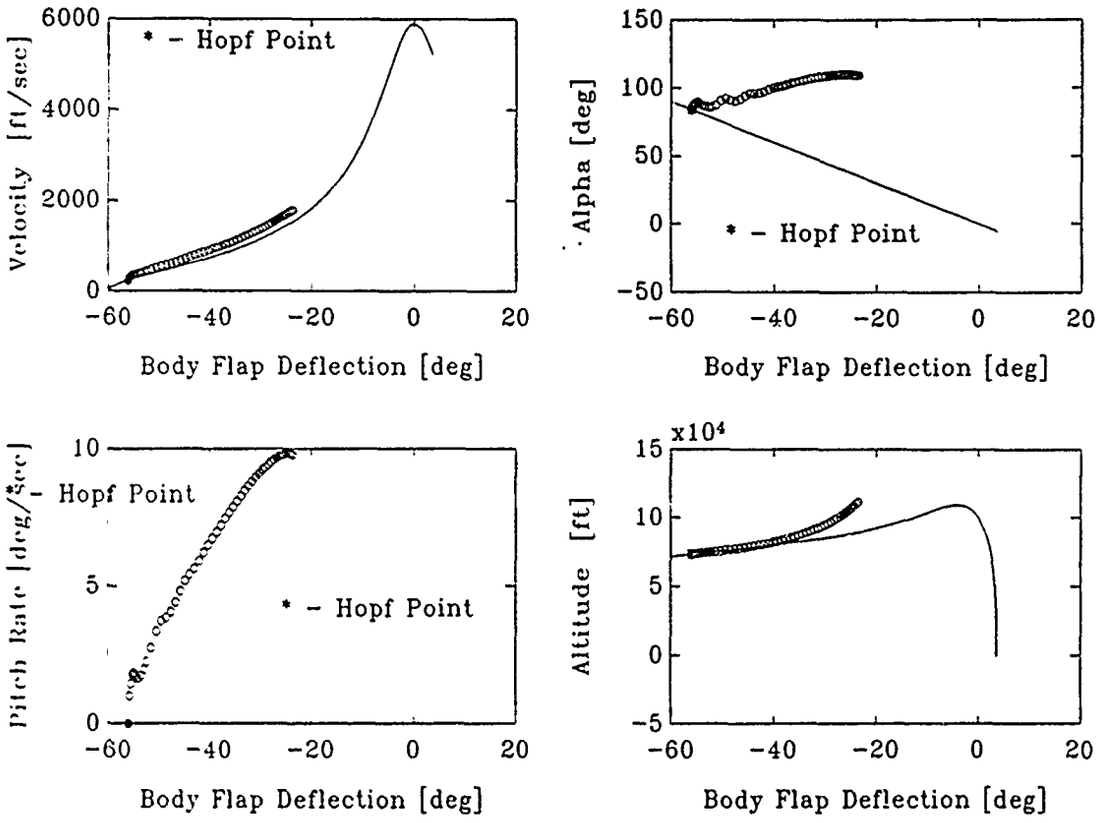

Figure 24. Partial Body Flap Sweep from 100 kft for the Air-Breathing engine case

Figure 25 shows the limit cycles over one period for a point near the Hopf bifurcation (δ_{bf} = -52.77° ; T = 77 sec) and the point on the end of the calculated periodic branch (δ_{bf} = -23.54° ; T = 140 sec). Clearly visible is the increase in nonlinear behavior as one moves along the periodic branch. Near the Hopf point one can see the motion is nearly constant and what little variation is there is sinusoidal. For points

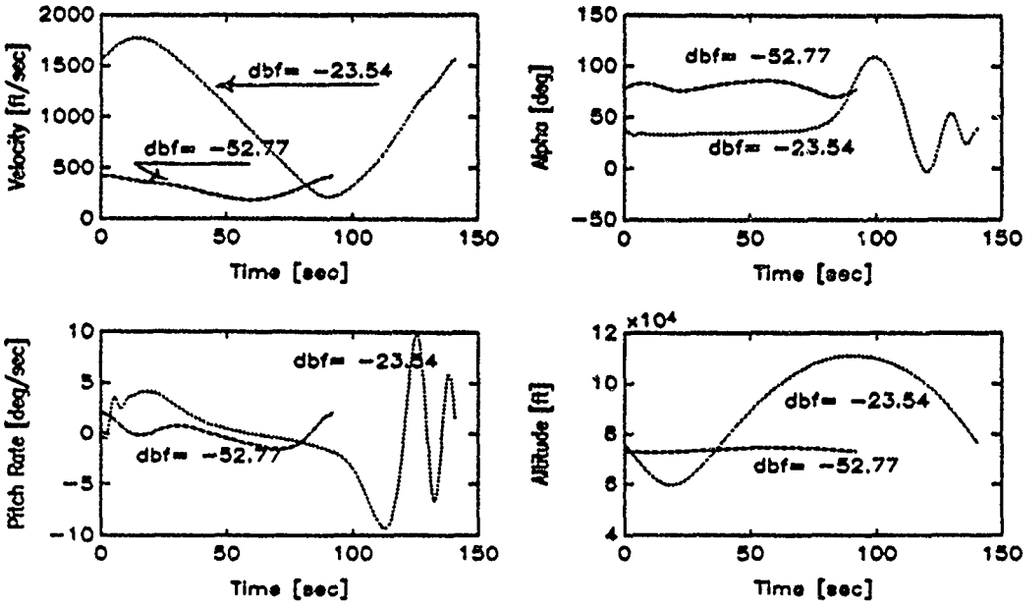

Figure 25. Limit Cycles for δ_{bf} = -52.77° & δ_{bf} = -20.54°, Body Flap Sweep from 100 kft : Air-Breathing Engine

farther along the periodic branch the nonlinear behavior, due to the underlying nonlinear equations, truly begins to blossom.

Figure 26 shows the limit cycles for δ_{bf} = -52.77° and -23.54° in the phase plane. Once again the classic phugoid-like behavior of the translational states is seen. Note as before in the constant thrust case the rotational states have this sub-oscillation. In contrast to what was seen in the constant thrust rocket case, here the phugoid mode has gone unstable at relatively low altitude (approximately 73,000 ft).

A body flap sweep from 400,000 ft for the air-breathing engine case is shown in Figure 27. The general characteristics for this sweep are the same as for the constant thrust rocket. However here the periodic branch remains unstable. As with the constant thrust rocket case, each equilibrium branch has a limit point where the height mode stabilizes.

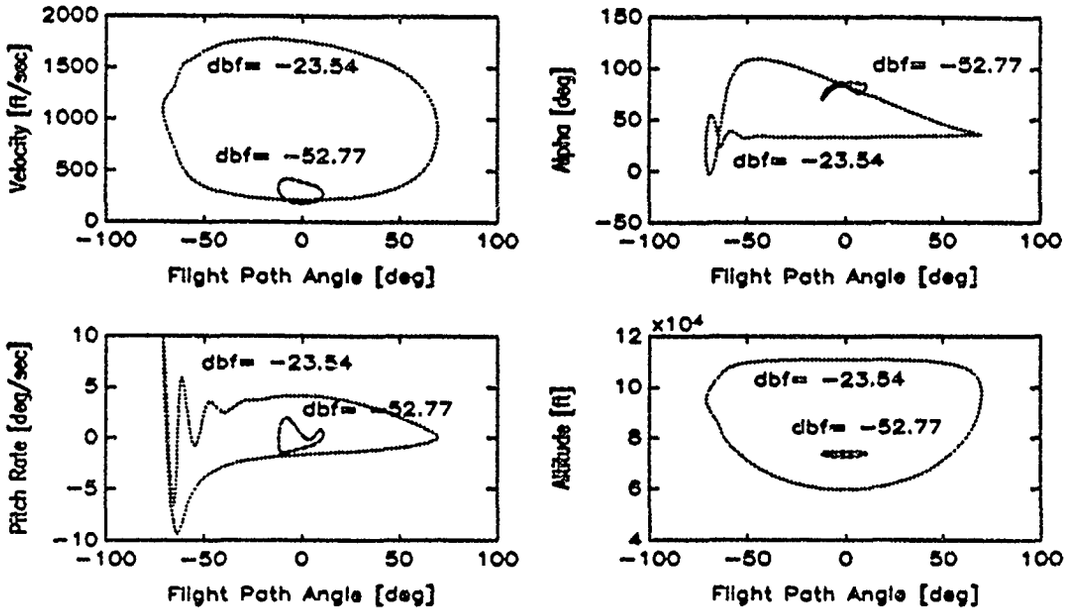

Figure 26. Limit Cycles in Phase Plane (δ_{bf} = -52.77° & -23.54°)
Body Flap Sweep from 100 kft : Air-Breathing Engine

There are also several limit points found along each periodic branch; just as with the constant thrust rocket body flap sweep from 400,000 ft.

Figures 28 and 29 show the limit cycles over one period and the limit cycles in the phase plane for the right periodic branch with δ_{bf} = -0.00078° and 0.0118°. Figures 30 and 31 show the limit cycles over one period and the limit cycles in the phase plane for the left periodic branch with δ_{bf} = -0.0046° and -0.011°. These points are as before, used to show the behavior of the limit cycle near the Hopf point versus the behavior farther down the periodic branch. The same basic behavior is seen for the translational states as discussed for previous cases. However of interest is the phase shift occurring along the left periodic branch. It is interesting to see how the left branch differs markedly from the right branch even though the two look relatively symmetric.

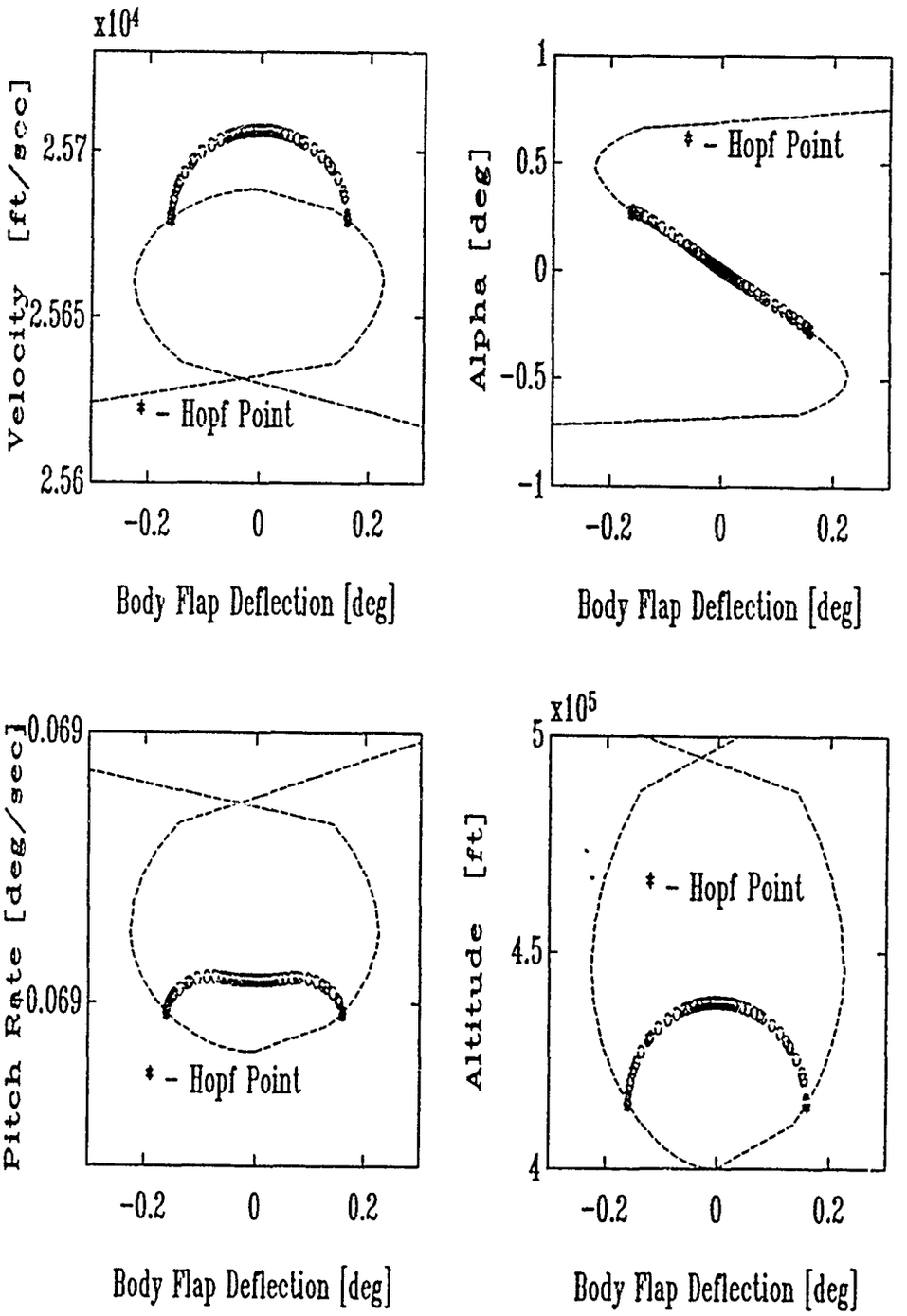

Figure 27. Collection of Bifurcation Diagram for Body Flap Sweep from 400 kft : Air-Breathing Engine Case

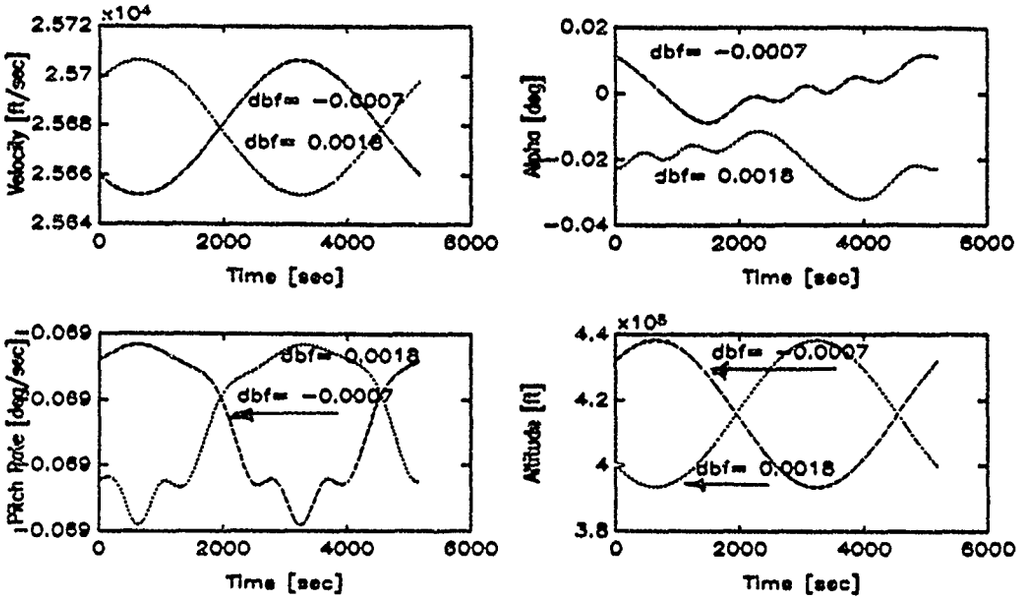

Figure 28. Limit Cycles over one Period δbf= -0.0007° and 0.0118° Body Flap sweep from 400 kft : Air-Breathing Engine Case

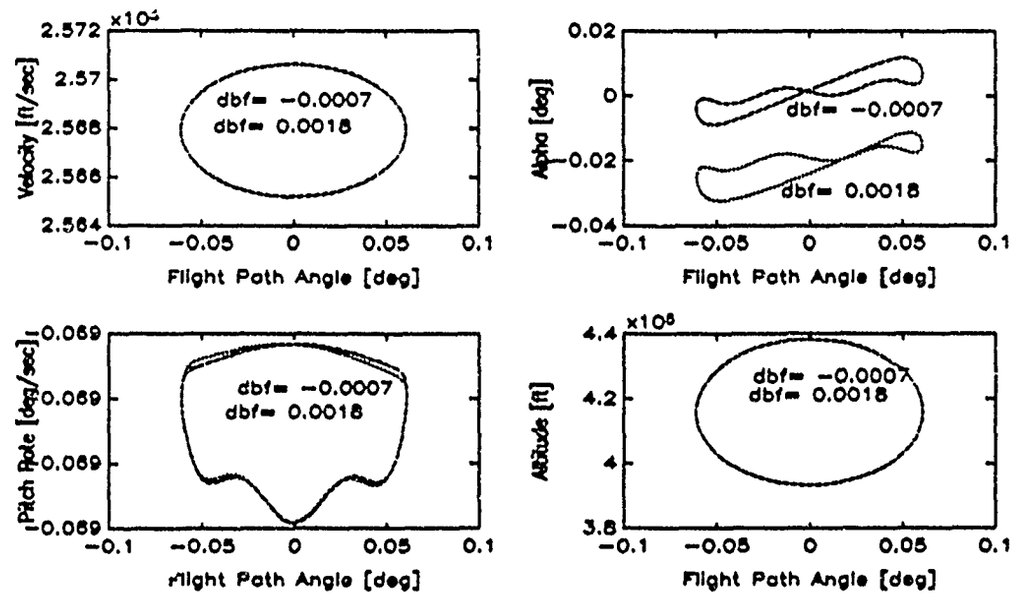

Figure 29. Limit Cycles in Phase Plane for δbf= -0.0007°and 0.0118° Body Flap Sweep from 400 kft : Air-Breathing Engine

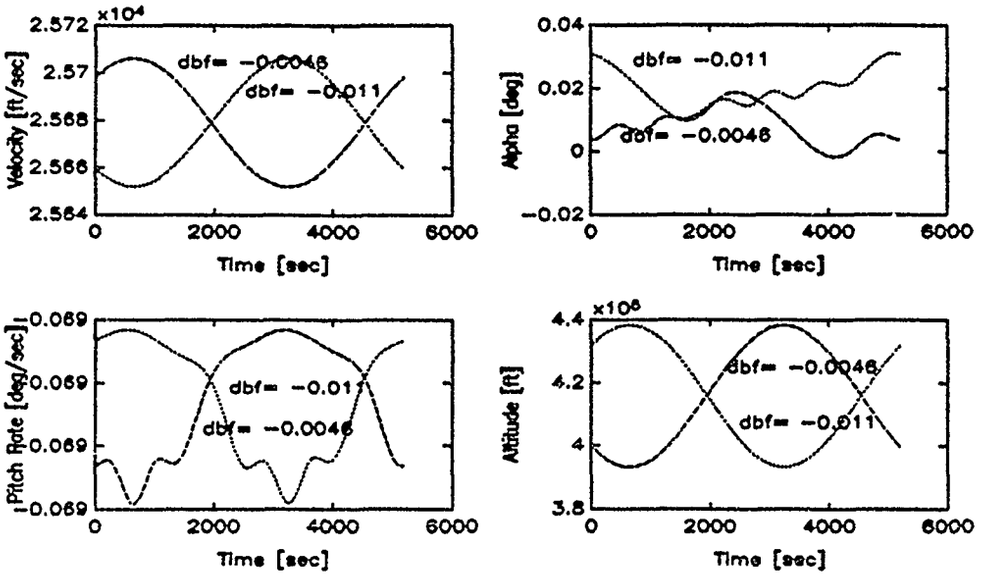

Figure 30. Limit Cycles, Left Branch, (δ_{bf} = -0.0046° & -0.011°) Body Flap Sweep from 400 kft : Air-Breathing Case

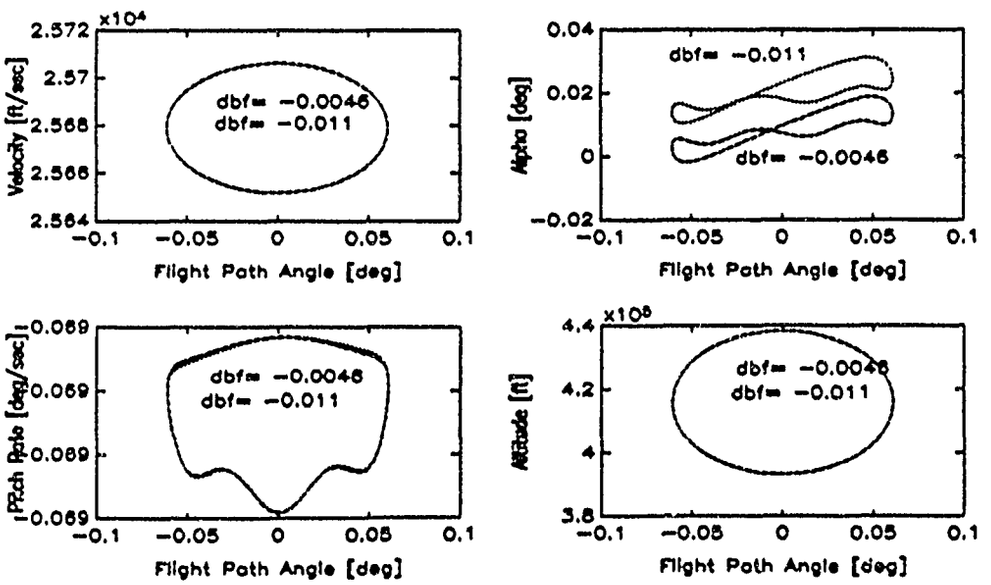

Figure 31. Limit Cycles in Phase Plane, Left Branch (δ_{bf} = -0.0046° & -0.011°), Sweep from 400 kft : Air-Breathing Engine

Throttle Parameter (δT) Variation

The throttle parameter acts as a multiplier to scale the equilibrium value of thrust. In the case of the constant thrust rocket it scales the value of the thrust at the starting altitude which was set equal to the drag. For the air-breathing engine case the throttle parameter scales the thrust as with the rocket case (i.e. which was set equal to drag at the starting altitude), however for the air-breathing case the thrust varies as a function of altitude via $T = T_0 [\rho(r)/\rho_0]$. A change in thrust causes a corresponding change in drag to maintain equilibrium so once again the velocity and radius begin to play an important role. However an interesting characteristic of the equilibrium solution paths where the throttle is the parameter is the lack of any modulation in the coefficient of lift or drag; which remain effectively constant at all throttle settings and radii.

The analysis using the throttle as a parameter was done in the very same manner as the body flap parameter. As before a starting altitude was selected (with $\alpha = \theta = 0$ radians) from which the equilibrium values for the remaining states were calculated. From this point the throttle parameter was first increased from $\delta T=1.0$ then decreased. This yielded a complete throttle sweep.

Constant Thrust Rocket Case. Not much happened with this case. From Figures 32 and 33 one can see the system is unstable, due to the height mode, and is nonlinear but no bifurcations were detected. It appears without the pitching associated with the body flap there is little to drive the nonlinear nature of the problem. In contrast to the cases where

the body flap was used as the parameter the angle of attack in these cases is basically zero.

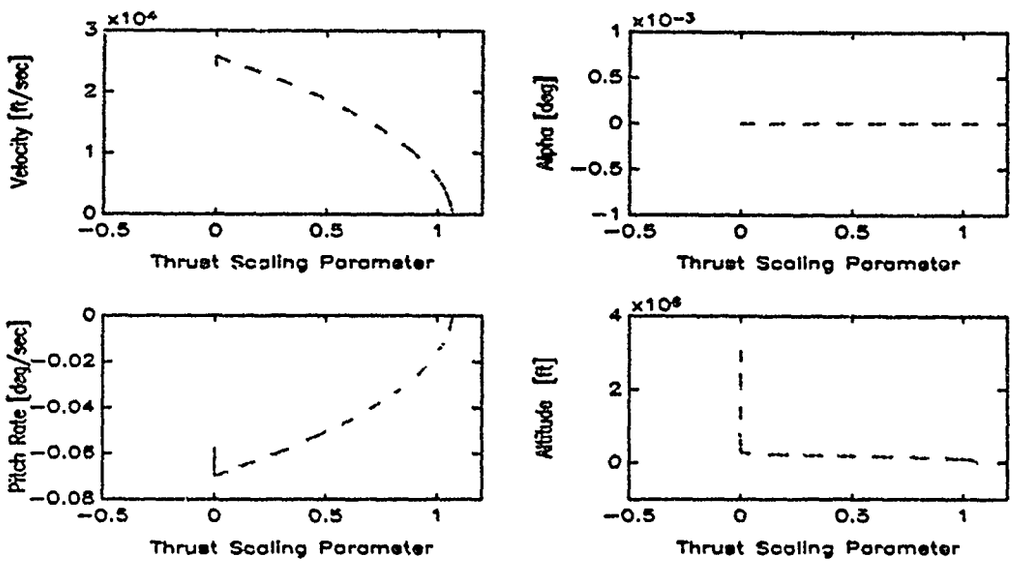

Figure 32. Collection of Bifurcation Diagrams for Throttle Sweep from 100 kft : Constant Thrust Rocket

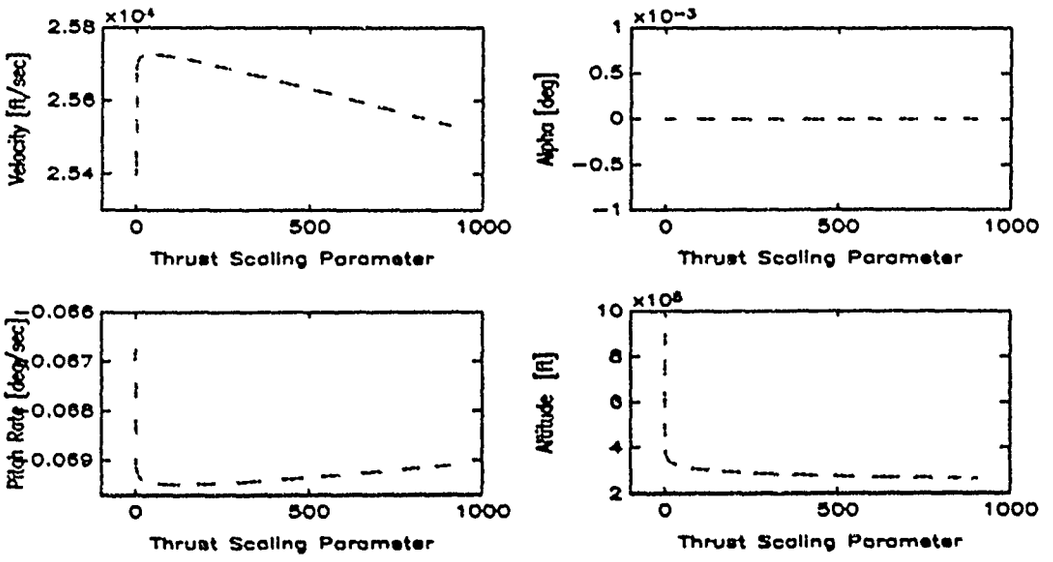

Figure 33. Collection of Bifurcation Diagrams for Throttle Sweep from 400 kft : Constant Thrust Rocket

Air-Breathing Engine Case. For the air-breathing case the most interesting behavior was at altitudes below 400,000 ft. The following discussion characterizes the general nature of what was found at these "lower" altitudes. Figure 34 shows the δT sweep for the air-breathing engine from 100,000 ft. For the portion of the sweep where $\delta T < 1.0$ the system remains stable. For the portion of the sweep where $\delta T > 1.0$ the system loses stability subcritically at a limit point ($\delta T = 18.99$) where the height mode crosses the imaginary axis. Just after this occurs ($\delta T = 18.93$) a Hopf Bifurcation point is found. Since the limit point preceded the Hopf point this bifurcation is not classified either supercritical or subcritical and as before is really of little physical value other than to perhaps give an idea of the bound on the allowable perturbation to remain in the vicinity of the equilibrium solution branch.

Figure 35 shows an expanded view of the area around the Hopf point and Figure 36 shows just the maximum limit cycles from the bifurcation diagram. These limit cycles show quite a variation of amplitude for the rotational states along the periodic branch as δT is increased. Looking at Figure 37 one sees smooth sinusoidal behavior in the translational states even though the limit cycles are for points well toward the end of the calculated portion of the periodic branch ($\delta T = 19.063$ and 19.078). The rotational states however, display some relatively high frequency sub-oscillations. Although the amplitudes of these sub-oscillations are quite small and the period is on the order of 150 seconds (see Figure 38). In examining the phase plane representations of the limit cycles versus the flight path angle (Figures 39 and 40) one sees the translational states clearly displaying the motion that can be associated with an elliptical orbit. Further support of this view is given from Figure 41, where the

variation in the overall parameter dependent period of the periodic branch is shown relative to the circular orbital period for the values of the states at the given δT.

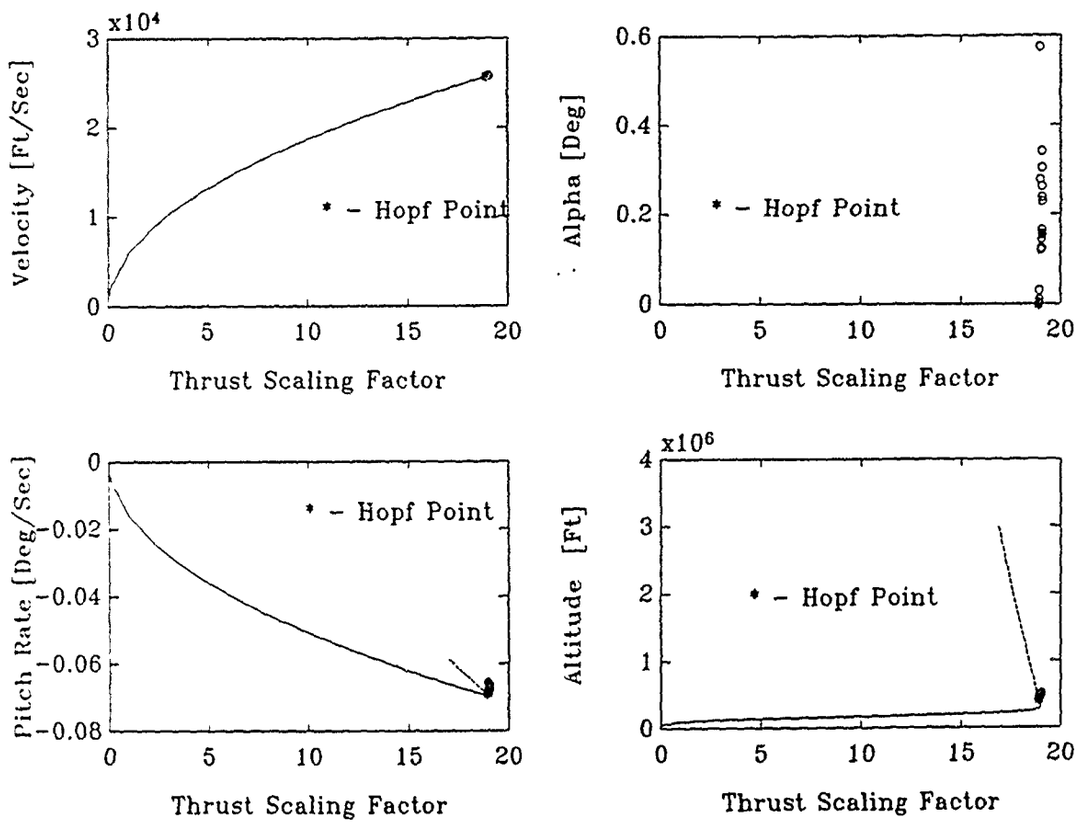

Figure 34. Collection of Bifurcation Diagrams for Throttle Sweep from 100 kft for Air-Breathing Engine Case

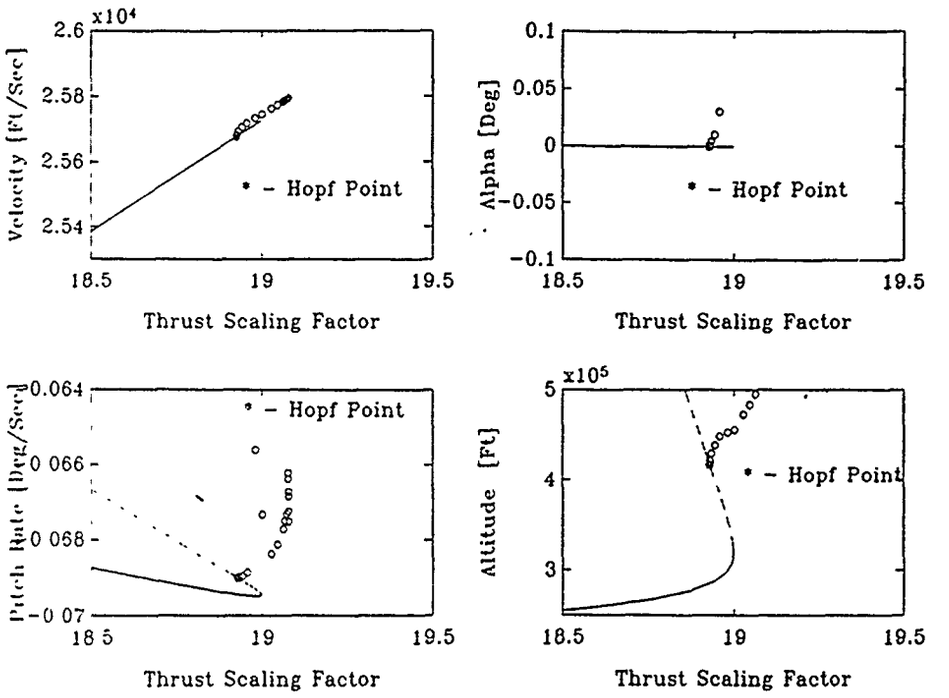

Figure 35. Expanded View of Region near Hopf Point for δT sweep from 100 kft for Air-Breathing Engine Case

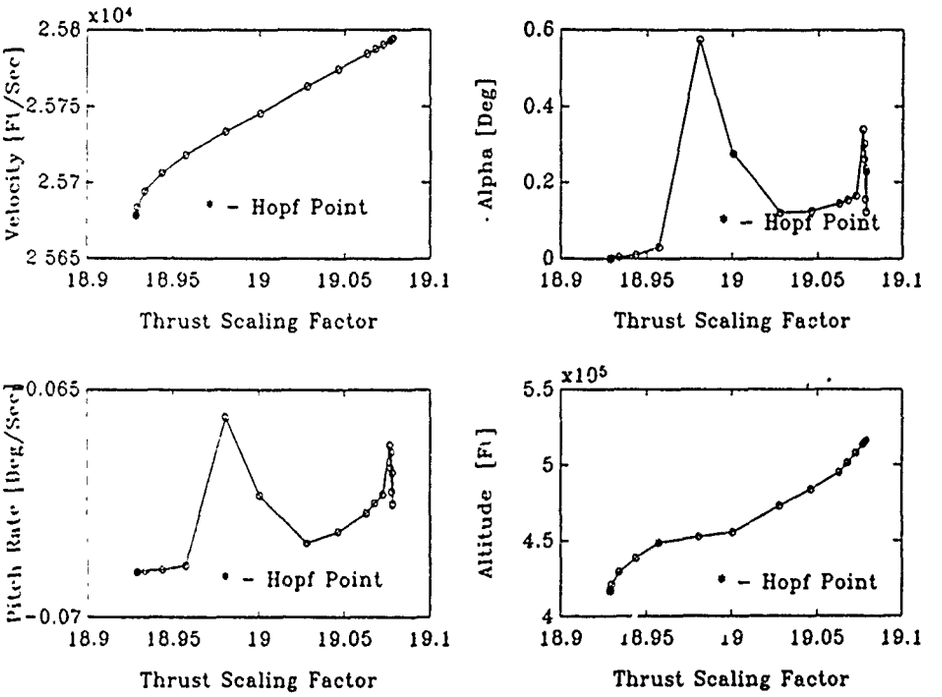

Figure 36. Maximum Limit Cycles for the δT sweep from 100 kft for Air-Breathing Engine Case

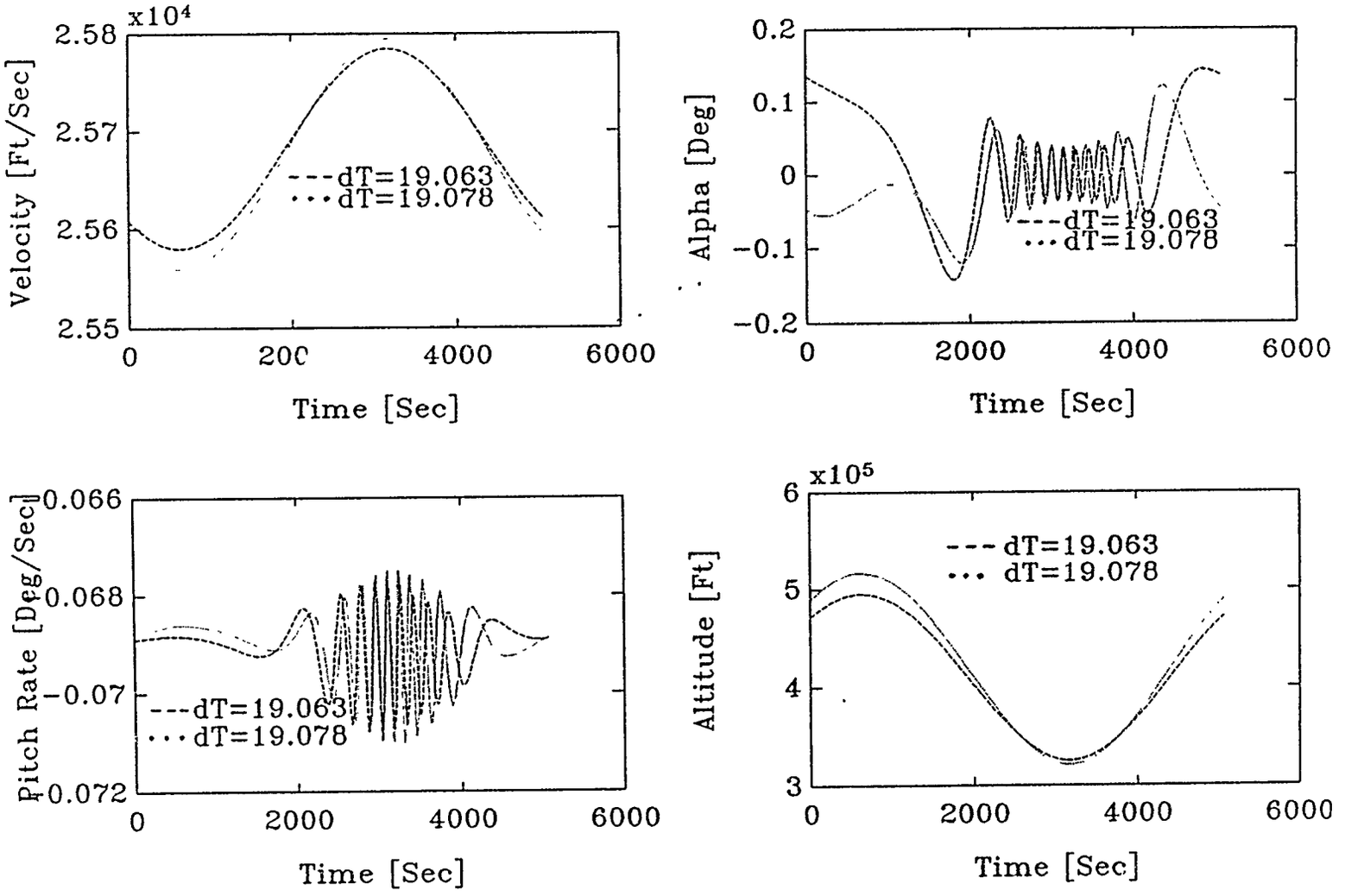

Figure 37. Limit Cycles over One Period for T = 19.06 & 19.07, Throttle Sweep from 100 kft Air-Breathing Engine

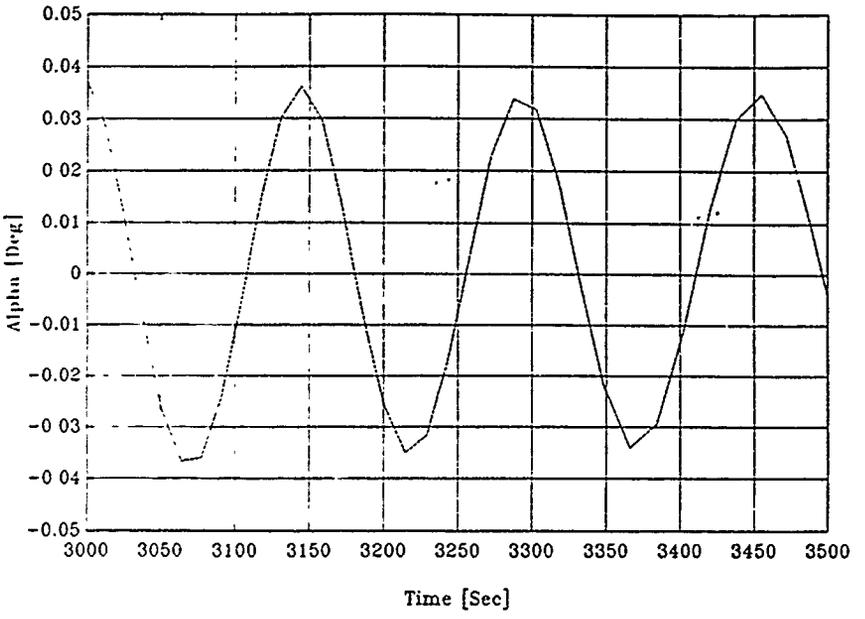

Figure 38. Expanded View of α Limit Cycle, δT = 19.063 Throttle Sweep from 100 kft : Air-Breathing Engine

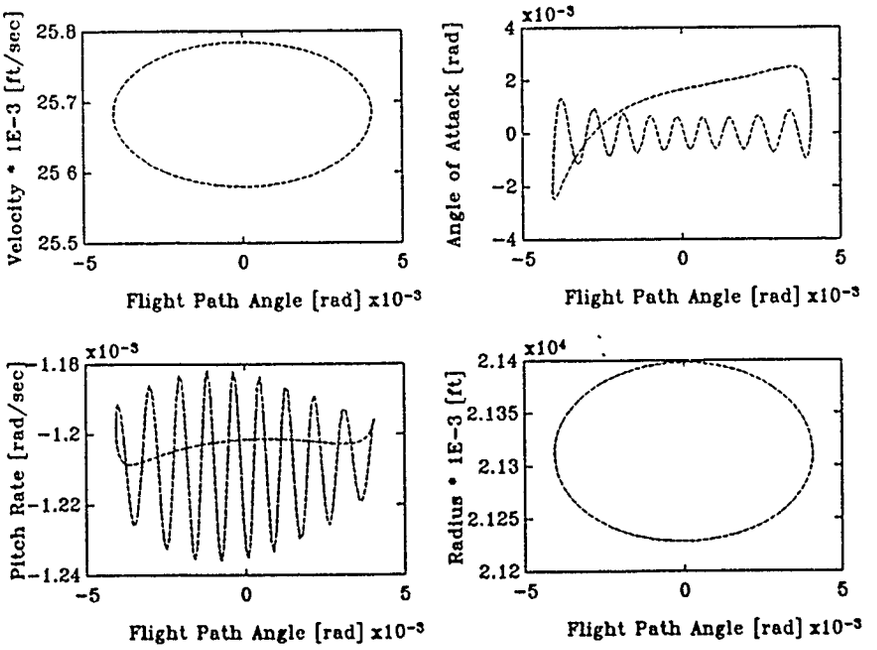

Figure 39. Limit Cycles in Phase Plane for δT = 19.063 Air-Breathing Engine Case from 100 Kft

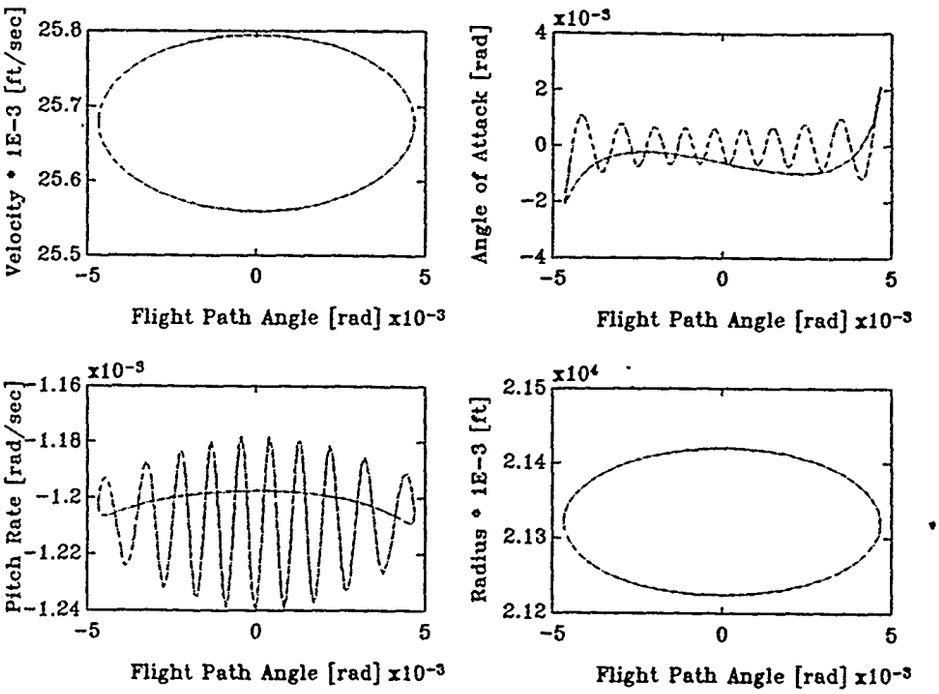

Figure 40. Limit Cycles in Phase Plane for δT = 19.078 Air-Breathing Engine Case from 100 kft

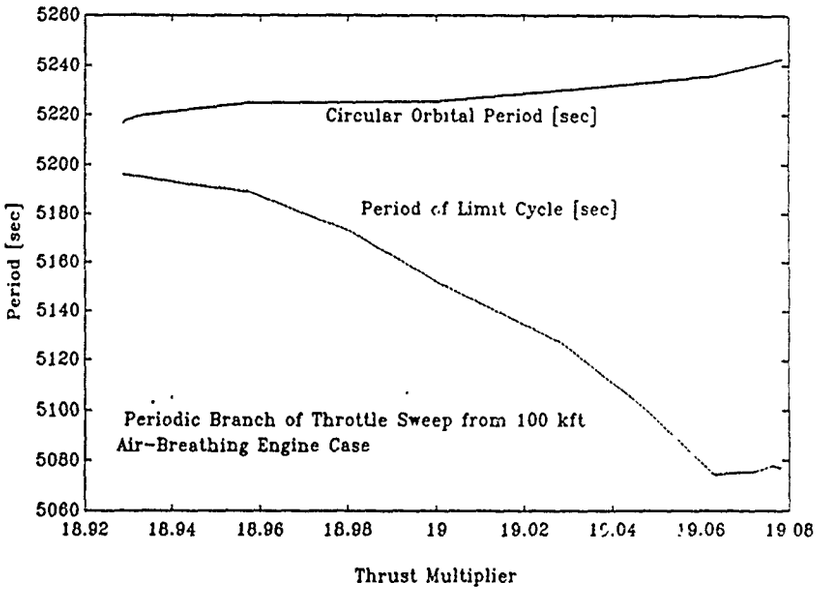

Figure 41. Comparison of Circular Orbital Period and Period of Limit Cycles for Throttle Sweep from 100 kft : Air-Breathing

IV. Model Stabilization

Simple Feedback Options

In Stengel's work (13) he presented a summary of several possible feedback schemes using several controls. Table 1 in section I is a reproduction of the table found in Stengel's paper. In looking at these possible schemes one becomes aware of the dichotomy regarding the height mode and the phugoid mode. Most stabilizing feedback for the height mode destabilizes the phugoid and vice versa. In Berry's work (2) similar feedback options were tried for the linear approximation technique and found to display the same behavior as found by Stengel. This "inverse" relationship between the height mode and the phugoid mode plus the restrictions imposed by the simplicity of the vehicle model made it beyond the scope of this thesis to actually stabilize the height mode. The success in stabilizing the height mode and not destabilizing the phugoid lay in developing a control law/technique to properly modify the way the longitudinal forces vary with height and velocity (as discussed in section I). Minor success was experienced in dealing with the phugoid by using pitch rate feedback to the body flap. It should be noted that pitch rate feedback in general has little affect on the phugoid roots however it was a technique that could be easily managed and did demonstrate the concept. For a given change in the pitch rate feedback the phugoid mode could be improved, but so slightly that in a practical sense it was worthless. Figure 42 shows the basic feedback loop with the pitch rate relative to the earth fed back in a negative feedback loop to the body flap (δ_{bf}).

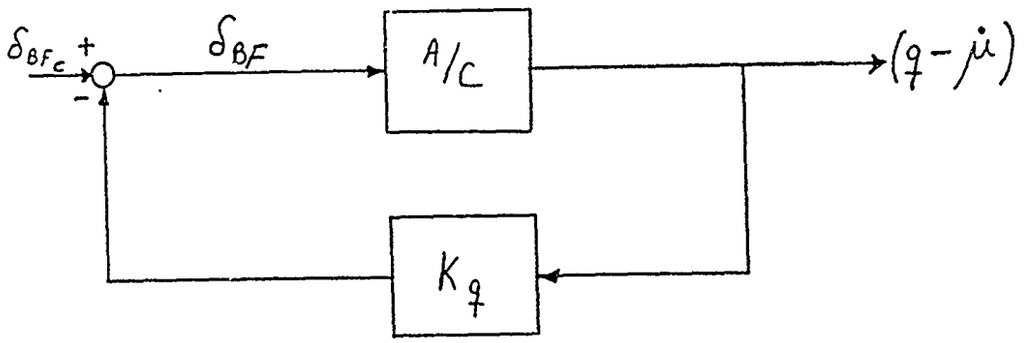

Figure 42. Pitch Rate Feedback Loop for Model Stabilization

Note the parameter now becomes the value input as the command (δ_{bfc}). The new value of δ_{bf} for use in eqn(22), the moment coefficient equation is given by the following:

$$\delta_{bf} = \delta_{bfc} - K_q (q - \dot{\mu}) \frac{360}{2\pi} \tag{40}$$

where: δ_{bfc} = new parameter for body flap sweep control (deg)
K_q = pitch rate feedback gain

Figure 43 is sufficiently representative of all the cases where pitch rate feedback was used. It must be emphasized that the curve in Figure 41 is a curve of Hopf bifurcation points. What can be seen is that as the value of Kq is changed the location of the Hopf point relative to the body flap deflection is changed. In this case a gain of Kq=20 pushes the Hopf point down the curve the farthest. However, as one can clearly see the improvement is extremely small; to the point of being basically

constant thrust rocket system and attempting to use alternative feedback of other states, it seems that without recasting the mathematical model to allow for more reasonable feedback control, say with attitude command inputs, significant stabilizing routines cannot be obtained.

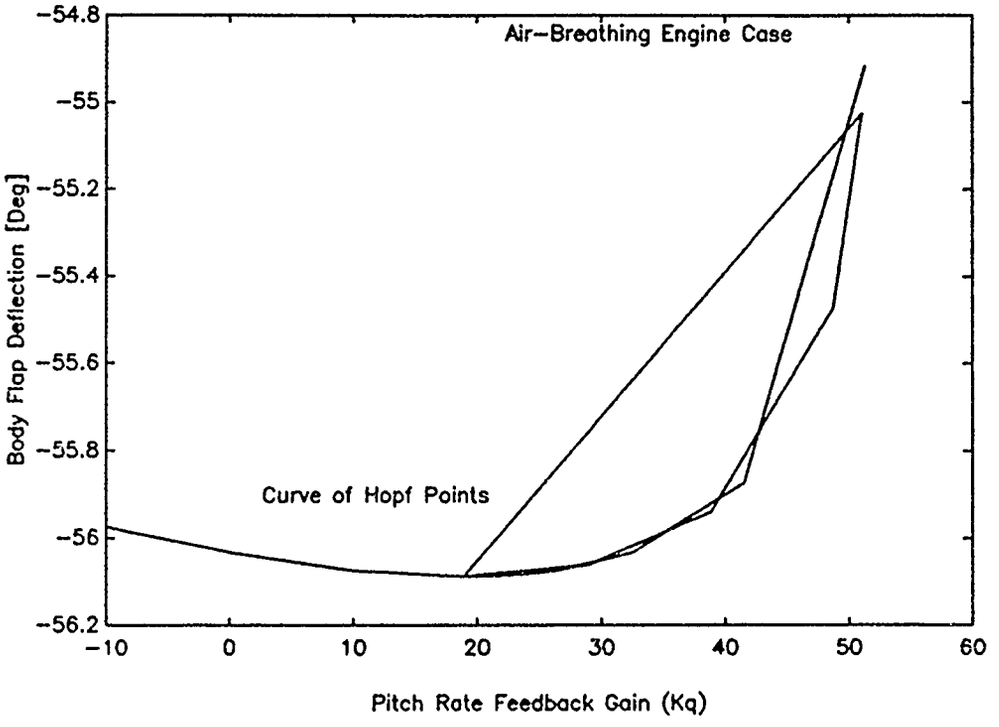

Figure 43. Movement of Hopf Bifurcation given Pitch Rate Feedback to the body flap. Air-Breathing Engine from 100 kft

V. Conclusions and Recommendations

Conclusions

Overall this study has not produced results that would be considered "Earth shaking" or significantly different from previous work. It has however resulted in some worthwhile accomplishments, not the least of which is demonstrating how easy it is to use bifurcation analysis on problems related to hypersonic flight. This method provided much the same information as obtained by other authors using perturbation techniques, yet gave a much greater view of the actual effects of the nonlinear nature of the problem.

In terms of comparison to previous work, it was found that the period and damping of the phugoid and pitching modes was similar to the behavior discovered by Vihn and Dobrzelecki and verified by Markopoulos, et al. (15:16-18; 7:286,287). Their study showed that the two modes do not cross for the linearized model as Etkin had concluded, but instead come very close together then diverge (4:785,786); this was the case here as well. From past work the behavior associated with the two modes in the vicinity of the "resonance altitude" (15;16) are expected to be coupled and behave nothing like that expected of the classic pitching and phugoid modes. It was shown here that there is significant departure from the classic behavior of the rotational states, in that they show significant motion when the phugoid mode goes unstable. However the translational states act basically as expected. Looking at the limit cycles of the periodic branch associated with the "resonance altitude" one sees what

could be described as a one way coupling from the translational states to the rotational states, with the rotational states experiencing sub-oscillating for each period of the translational states. In addition the loss of stability at high altitude which Etkin concluded would occur due to the loss of pitch damping and a destabilizing moment due to the effect of the gravity gradient was seen (4:785,787).

For the body flap bifurcation analysis the most interesting findings are the results associated with the nonlinear behavior around 400,000 ft starting altitude. Of note in this analysis is the very marginal instability or stability that may exist in this region. In all cases the real part of the eigenvalues are very near the imaginary axis when in this altitude region. In the case of the constant thrust rocket starting at 400,000 ft, the periodic branch was found to have a region of stability. This implies that trajectories within a relatively small domain of attraction would be drawn to the limit cycle therefore the vehicle could expect to experience stable periodic motion, on the order of the orbital period, with fairly significant amplitude for velocity and altitude. Looking at the behavior of the translational states and given that the period of the limit cycle is nearly equal to that of a circular orbit, it seems likely that the limit cycles associated with the "resonance altitude" describe the velocity and altitude of an elliptical orbit.

The bifurcation sweeps using the throttle parameter showed for the most part that the throttle is a very benign way to control the energy of the vehicle. Little was found that was of physical interest from the stand point of examining nonlinear behavior. The most interesting behavior was found for the air-breathing case with starting altitudes below 400,000 ft. At these "lower" altitudes the higher atmospheric

density made the aerodynamic forces more effective and the equilibrium energy management is done by changing velocity and altitude without rotating the vehicle. Only one physically realistic Hopf point was found for these low altitude sweeps. The periodic motion looked similar to that obtained from the body flap sweeps in terms of the altitude and velocity, however the rotational states experience a relatively high frequency sub-oscillations relative to what was seen before. In further comparing the results to the bifurcation sweeps using the throttle parameter and the body flap parameter for the constant thrust rocket case the pitch angle and the variation of the lift coefficient play key roles in the dynamics of the system. It seems without the pitch angle providing the impetus for instability the Hopf bifurcation at high altitudes where aerodynamic pitch damping is lost is not seen, which is not altogether surprising.

Augmenting the vehicle model to obtain system stability for cases where the height mode is unstable seems to be intractable without changing the model to allow for commanded attitude input and the ability to generate or obtain the measurements of states or some value associated with a state that will allow for the minimization of some error.

Certainly the rich dynamics associated with nonlinear phenomena has been demonstrated by the resulting complex behavior present even in this simple example. This work stands in contrast to those in previous studies who claimed to have explored the nonlinear nature of the longitudinal dynamics of a powered lifting hypersonic vehicle by simply including second order terms in the Taylor series expansions for small perturbation analysis. While no great departures of physical significance were found in this study from that which was previously obtained by others, this work does display many of the major findings of previous works and adds insight

to the expected local behavior of trajectories.

Perhaps most useful of all, is this work displays the tremendous utility and encompassing nature of bifurcation analysis as well as the ease with which it can be applied to problems of this sort.

Recommendations

This work really stands as a first step. It opens the door to a variety of areas for further investigation. Several of these are briefly mentioned below.

1. Add the lateral equations of motion and study the dynamics of a powered lifting hypersonic vehicle flying a minor circle. This would provide significant coupling of the longitudinal and lateral dynamics and should make for some interesting behavior.
2. Define the aerodynamic forces and moment coefficients in nonlinear terms as found in references such as Etkin's text (5:199,393).
3. Include the rotation of the Earth in the equations of motion.
4. Increase the accuracy of the thrust laws to reflect more up-to-date propulsion concepts such as ramjets and scramjets. This would bring Mach number and additional altitude dependencies.
5. Develop higher order control systems to stabilize the height mode without destabilizing the phugoid mode. This will require the addition of states to the model to allow for commanded attitudes and feedback to controls with direct influence over altitude and velocity. Recall for this study the simple feedback of available states to the body flap proved worthless for stabilizing the height mode and of little value in maintaining phugoid stability much beyond an original Hopf point.

Appendix A: FORTRAN Listing of the User Supplied Subroutines for AUTO

```
C         CURRENT AS OF 23 Nov 1990
C-----------------------------------------------------------------------
C-----------------------------------------------------------------------
C-----------------------------------------------------------------------
C-----------------------------------------------------------------------
C
      SUBROUTINE FUNC(NDIM,U,ICP,PAR,IJAC,F,DFDU,DFDP)
C     ---------- ----
C
C This subroutine evaluates stationary solutions from the equations of
C motion for a powered lifting aerospace vehicle flying along a great
C circle about a nonrotating spherical Earth.
C Input parameters :
C       NDIM   -   Dimension of U and F.
C       U      -   State Vector containing U.
C                  U(1)= V/V0 the velocity along the flight path divided
C                        by a constant (nondimensional)
C                  U(2)= alpha   Angle of Attack [radians]
C                  U(3)= q       Pitch Rate of the Body relative
C                                 to the Earth [rad/sec]
C                  U(4)= theta   Pitch Angle  [radians]
C                  U(5)= r/R0    Radius from Earth's Center divided by a
C                                 constant (nondimensional)
C       PAR    -   Array of parameters in the differential equations.
C       PAR(1) = df     Body Flap deflection  [degrees]
C       ICP    -   PAR(ICP(1)) is the initial 'free' parameter.
C       IJAC   -   =1 if the Jacobians DFDU and DFDP are to be returned,
C                  =0 if only F(U,PAR) is to be returned in this call.
C
C Values to be returned :
C       F      -   F(U,PAR)  the right hand side of the ODE.
C       DFDU   -   The derivative (Jacobian) with respect to U.
C
C
      IMPLICIT DOUBLE PRECISION (A-H,O-Z)
      DOUBLE PRECISION L,K0,Ky,mslug,Lift
C
      DIMENSION U(NDIM),PAR(20)
      DIMENSION F(NDIM),DFDU(NDIM,NDIM),DFDP(NDIM,20)
      COMMON /CNST/ alt,L,Ky,K0,re,R0,V0,gs,IRSTST,ITEST
      COMMON /FUNVL/ rho,g,Cd,Cl,CM,TPM,DRODU5,DGDU5,S,mslug
      COMMON /AERO/ Cd0,Cda,Cl0,Cla,CM0,CMa,CMdf,CMq
      COMMON /CFORC/ orbper,Drag,Lift,altw,W,Fc,Tx,Ty
C
C..... Set flag for Subroutine Const to use current values
C..... of the States rather than initial values.
C
       ITEST=0
C
C..... Call Subroutine CONST to obtain the States, plus the
C..... necessary constants and functional values
C
       CALL CONST(U)
C
C*************************************************************************
C************** System of 5 Nonlinear Equations of Motion ****************
C*************************************************************************
C
C..... dV/dt  SCALED ie U(1)= V/V0 (Note U(1) is nondimensional)
C..... NOTE: TPM = T/m
```

```
C
      F(1)=( (TPM)*DCOS(U(2)) - (0.5D0*rho*S*Cd*(V0*U(1))**2)/mslug
     &     -g*(DSIN(U(4))*DCOS(U(2))-DCOS(U(4))*DSIN(U(2))) ) / V0
C
C..... d(alpha)/dt
C
      F(2)=U(3)+( g/(U(1)*V0) )*(DCOS(U(4))*DCOS(U(2))+DSIN(U(4))
     &      *DSIN(U(2)))-(TPM/(U(1)*V0))*DSIN(U(2))-
     &      (0.5D0*rho*S*Cl*U(1)*V0/mslug)
C
C..... dq/dt
C
      F(3)=( (0.5D0*rho*S*L*CM*(U(1)*V0)**2) / (mslug*Ky**2) )
     &     -( (1.5D0)*( g/(U(5)*R0) )*(K0)*DSIN(2.0D0*U(4)) )
C
C..... d(theta)/dt
C
      F(4)=U(3)+( ( (U(1)*V0)/(U(5)*R0) )*( DCOS(U(4))*DCOS(U(2))+
     &DSIN(U(4))*DSIN(U(2)) ) )
C
C..... dr/dt
C
      F(5)=((U(1)*V0)/R0)*(DSIN(U(4))*DCOS(U(2))-
     &               DCOS(U(4))*DSIN(U(2)))
C
       IF(IJAC.EQ.0)RETURN
C
C
      RETURN
      END
C
      SUBROUTINE STPNT(NDIM,U,PAR)
C     ---------- -----
C
C..... In this subroutine the steady state starting point must be defined.
C..... (Used when not restarting from a previously computed solution).
C..... The problem parameters (PAR) may be initialized here or else in INIT.
C
C       NDIM   -   Dimension of the system of equations.
C       U      -   Vector of dimension NDIM.
C                  Upon return U should contain a steady state solution
C                  corresponding to the values assigned to PAR.
C       PAR    -   Array of parameters in the differential equations.
C
      IMPLICIT DOUBLE PRECISION (A-H,O-Z)
      DOUBLE PRECISION L,K0,Ky,mslug
C
      DIMENSION U(NDIM),PAR(20)
      COMMON /CNST/ alt,L,Ky,K0,re,R0,V0,gs,IRSTST,ITEST
      COMMON /FUNVL/ rho,g,Cd,Cl,CM,TPM,DRODU5,DGDU5,S,mslug
      COMMON /AERO/ Cd0,Cda,Cl0,Cla,CM0,CMa,CMdf,CMq
C
C..... Initialize the problem parameters.
C
        PAR(1)=0.0D0
        write(*,*) 'Enter initial par(2)=Kq and par(3)=W/S
     & par(4)= Trho, and par(5)=throttle'
        read(*,5)PAR(2)
        read(*,5)PAR(3)
        read(*,5)PAR(4)
```

```
        read(*,5)PAR(5)
 5      format(d15.6)
        U(2)=0.0D0
        U(4)=0.0D0
        ITEST=10
        CALL CONST(U)
C
      RETURN
      END
C
      SUBROUTINE INIT
C     ---------- ----
C
C..... In this subroutine the user should set those constants that require
C..... values that differ from the default values assigned in DFINIT.
C..... (See the main documentation for the default assignments).
C
      IMPLICIT DOUBLE PRECISION (A-H,O-Z)
C
      COMMON /BLBCN/ NDIM,IPS,IRS,ILP,ICP(20),PAR(20)
      COMMON /BLCDE/ NTST,NCOL,IAD,ISP,ISW,IPLT,NBC,NINT
      COMMON /BLDLS/ DS,DSMIN,DSMAX,IADS
      COMMON /BLLIM/ NMX,NUZR,RL0,RL1,A0,A1
      COMMON /BLMAX/ NPR,MXBF,IID,ITMX,ITNW,NWTN,JAC
C
C*********************************************************************
C****************** READ AUTO PARAMETERS ***************************
C*********************************************************************
C
       OPEN(UNIT=27,FILE='DS.DAT',STATUS='OLD')
       REWIND (27)
C..... ITEMS IN COMMON BLBCN  - BASIC CONSTANTS
       READ(27,*) NDIM
       READ(27,*) IPS
       READ(27,*) IRS
       READ(27,*) ILP
       READ(27,*) ICP(1)
       write(*,*) 'Which parameter to vary?(PAR(2)=Kq PAR(3)=W/S
     &  PAR(4)=Trho, PAR(5)=Throttle setting)'
        read(*,5) I
 5      format(I1)
         ICP(2)=I
C..... ITEMS IN COMMON BLCDE - DISCRETIZATION CONSTANTS
       READ(27,*) NTST
       READ(27,*) NCOL
       READ(27,*) IAD
       READ(27,*) ISP
       READ(27,*) ISW
       READ(27,*) IPLT
C..... ITEMS IN COMMON BLDLS - STEPSIZE ALONG SOLN BRANCHES
       READ(27,*) DS
       READ(27,*) DSMIN
       READ(27,*) DSMAX
       READ(27,*) IADS
C..... ITEMS IN COMMON BLLIM - LIMITS
       READ(27,*) NMX
       READ(27,*) NUZR
       READ(27,*) RL0
       READ(27,*) RL1
       READ(27,*) A0
```

```
       READ(27,*) A1
C..... ITEMS IN COMMON BLMAX - MAXIMA
       READ(27,*) NPR
       READ(27,*) MXBF
       READ(27,*) IID
       READ(27,*) ITMX
       READ(27,*) ITNW
       READ(27,*) NWTN
       READ(27,*) JAC
       CLOSE (27)
C
      RETURN
      END
C
       FUNCTION USZR(I,NUZR,PAR)
C      -------- ----
C
C..... This subroutine can be used to obtain plotting and restart data
C..... at certain values of free parameters.
C
      IMPLICIT DOUBLE PRECISION (A-H,O-Z)
       DOUBLE PRECISION L,Ky,K0,mslug
C
      DIMENSION U(5),PAR(20)
      COMMON /CNST/ alt,L,Ky,K0,re,R0,V0,gs,IRSTST,ITEST
      COMMON /FNVL/ rho,g,Cd,Cl,CM,TPM,DRODU5,DGDU5,S,mslug
C
C..... Initially, for the steady state analysis, set NUZR=0 in INIT.
C..... Then the functions specified below will be ignored.
C
C..... When computing the branch of periodic solutions, set NUZR=4 in INIT.
C..... Output will then be written in unit 8 for the values
C..... of PAR(*) specified below.
C..... Note that PAR(11) is normally reserved. It is used by AUTO to keep
C..... track of the period (See main documentation).
C
      GOTO(1,2,3,4)I
C
 1     USZR=PAR(11) - 10.0
       RETURN
C
 2     USZR=PAR(11) - 14.0
       RETURN
C
 3     USZR=PAR(11) - 20.0
       RETURN
C
 4     USZR=PAR(11) - 30.0
       RETURN
C
      END
C
      SUBROUTINE CONST(U)
C     ---------- ------
C
      IMPLICIT DOUBLE PRECISION (A-H,O-Z)
      DOUBLE PRECISION L,K0,Ky,Lift,mdot,m,mslug
C
      DIMENSION U(NDIM)
      COMMON /BLBCN/ NDIM,IPS,IRS,ILP,ICP(20),PAR(20)
```

```
      COMMON /CNST/ alt,L,Ky,K0,re,R0,V0,gs,IRSTST,ITEST
      COMMON /FUNVL/ rho,g,Cd,Cl,CM,TPM,DRODU5,DGDU5,S,mslug
      COMMON /AERO/ Cd0,Cda,Cl0,Cla,CM0,CMa,CMdf,CMq
      COMMON /CFORC/ orbper,Drag,Lift,altw,W,Fc,Tx,Ty
C
C*****************************************************************************
C************** Aerodynamic and Geometric Constants **************************
C*****************************************************************************
        Cd0=0.0133D0
        Cda=0.4D0
        Cl0=0.05D0
        Cla=0.5D0
        CM0=0.0D0
        CMa=-0.0548D0
        CMdf=CMa*1.5D0
        CMq=-0.028D0
C
C...... Characteristic Length of Vehicle - overall length L=50 ft
C
        L=50.0D0
C...... Weight, Mass and Area of Vehicle
C
        Wsl=700.0D3
        S=Wsl/PAR(3)
        mslug=Wsl/32.174D0
C
C...... Radius of gyration in pitch [ft] - Ky^2 = Iy/m
C
        Ky=25.0D0
C
C...... K0=(Ix-Iz)/Iy
C
        K0=-0.94D0
C
C...... Radius of the Earth [ft] (standard geoid)
C
        re=2.0903264468D7
C
C...... Gravity at Earth's surface [ft/sec^2]
C
        gs=32.174D0
C
        V0=1000.0D0
        R0=1000.0D0
        raddeg=2.0D0*3.14159265359D0/360.0D0
C
C *****************************************************************************
C ************ READ ALTITUDE AND SET INITIAL U(5) ****************************
C *****************************************************************************
C
        IF(ITEST .GT. 5) THEN
          OPEN(UNIT=25,FILE='ALT.25',STATUS='OLD')
          REWIND (25)
          READ(25,*) alt
C
C...... SET INITIAL VALUE FOR THE RADIUS U(5).  NOTE: SCALED DOWN BY R0
C
          U(5)=(re+alt)/R0
C
        END IF
```

```
C
C*************************************************************************
C************** Density and Gravity variation with altitude ***************
C*************************************************************************
C
      IF( (U(5)*R0 - re) .LT. 6.0D5 ) THEN
C
C...... Convert altitude to SI units [km]
C
        altsi=( ( U(5)*R0 - re ) / 3.2808399D0 ) / 1000.0D0
C
C...... Calculate the density in SI units [Kg/m^3]
C...... Constants used in polynomial (U.S. Standard Atmosphere Supp. 1966)
C
       C0=0.1000000000D+01
       C1=0.3393495800D-1
       C2=-0.3433553057D-2
       C3=0.5497466428D-3
       C4=-0.3228358326D-4
       C5=0.1106617734D-5
       C6=-0.2291755793D-7
       C7=0.2902146443D-9
       C8=-0.2230070938D-11
       C9=0.1010575266D-13
       C10=-0.2482089627D-16
       C11=0.2548769715D-19
C
      eqn1=C0+(C1*altsi)+(C2*altsi**2)+(C3*altsi**3)+(C4*altsi**4)+
     &(C5*altsi**5)+(C6*altsi**6)+(C7*altsi**7)+(C8*altsi**8)+
     &(C9*altsi**9)+(C10*altsi**10)+(C11*altsi**11)
C
       rhoSI=1.2250D0/eqn1**4
C
C...... Convert from Kg/m^3 to Lbm/Ft^3
C...... (0.062427961 (lbm/ft^3)/(Kg/m^3) )
C
       rho=rhoSI*0.062427961D0
C
C...... Convert to [Slugs/ft^3]
C
       rho=rho/32.174D0
C
      ELSE
C
C...... Equation for rho if altitude is greater than 600,000 ft
C
         rho= 2.16871253724D-10 *
     &              DEXP(-8.89837671693D-6 * (U(5)*R0 - re) )
C
      END IF
C
C...... Calculate the gravitational acceleration
C
        g= gs * ( re / (U(5)*R0) )**2
C
C...... Calculate the Atmospheric Pressure
*        p0=2116.22D0
*        p1=-5.850746831820396D-05
*        p2=9.792179784448163D-01
*        p3=9.875326461241002D-05
```

```
*        p4=-6.044333173347913D-06
*        p5=3.408653276857509D-09
*        p6=-8.934489792146698D-07
*        alt=(U(5)*R0 - re)
*         Pa=p0*DEXP(p1*alt**p2)+p3*DEXP(p4*alt)+p5*DEXP(p6*alt)
C
C*************************************************************************
C******* Thrust Equations and Aerodynamic Coefficients *******************
C*************************************************************************
C
        Cd=Cd0+Cda*U(2)**2
        Cl=Cl0+Cla*U(2)
C
C...... Exhaust Nozzle Area [ft^2]
*         An=40.0D0
C
C...... Exhaust Velocity (Vexh) = 500 ft/sec
C
*         Vexh=500.0D0
C
C...... Rocket with constant Thrust at reference altitude and velocity.
C...... Note:  W/S=30 [lb/ft^2] at sea level, therefore
C...... U(1)initial = sqrt( (g r) / (1 + (rho r Cl S)/2m)) is
C
        IF (ITEST .gt. 5) THEN
C
           U(1)= DSQRT( (g*U(5)*R0)/( 1.0D0+(rho*S*U(5)*R0*Cl)/
     &                  (2.0D0*mslug) ) )
C
           U(3) = -U(1)/(U(5)*R0)
C
C...... Thrust Constant
C
           T0=( 0.5D0*rho*S*Cd*U(1)**2 )/(rho**PAR(4))
            write(*,*) 'T0=',T0
C
C...... Mass flow rate in [slugs/sec]
C
C...... Assume the Pressure is expanded to the starting altitude value
*            Pe=Pa
*            mdot=( (0.5D0*rho*(U(1)**2)*Cd*S) - (Pe-Pa)*An ) / Vexh
*          write(*,*) 'MDOT=',mdot
C
C...... SCALE DOWN U(1) and nondimensionalize
C
           U(1)=U(1)/V0
C
C...... PRINT RESTART DATA FILE
           OPEN(27,FILE='REF.DAT',STATUS='NEW')
           WRITE(27,10) alt,T0
 10        FORMAT(40x,'REFERENCE VALUES',/,6X,'ALT [FT]',
     &          14X,'T0 [ft^4/sec^2]',/,2(1X,E15.8,4X))
           CLOSE(27)
           OPEN(40,FILE='THRUST.DAT',STATUS='NEW')
           OPEN(41,FILE='COEFF.DAT',STATUS='NEW')
           WRITE(40,21)
           WRITE(41,22)
           IRSTST=10
           try=0.0d0
        ELSEIF (IRSTST .LT. 5) THEN
```

```
            OPEN(27,FILE='REF.DAT',STATUS='OLD')
            REWIND(27)
            READ(27,20) xjnk1,T0
            OPEN(40,FILE='THRUST.DAT',STATUS='NEW')
            OPEN(41,FILE='COEFF.DAT',STATUS='NEW')
            WRITE(40,21)
            WRITE(41,22)
 20         FORMAT(/,/,2(1X,E15.8,4X))
 21         FORMAT(6X,'H',15X,'Tx',15x,'D',15x,'Ty',15x,'L',15x,'W',
     &              15x,'Fc',14x,'Orb Per')
 22         FORMAT(8X,'H',15x,'Cl',15x,'Cd',15x,'CM',15x,'V',15x,
     &             'alpha',15x,'Rad')
            IRSTST=10
          END IF
C
           Thrust = (T0*rho**PAR(4)) * PAR(5)
           orbper= (6.2831853072D0 * U(5)*R0)/DSQRT(g*U(5)*R0)
           Drag= 0.5D0*rho*S*Cd*(U(1)*V0)**2
           Lift= 0.5D0*rho*S*Cl*(U(1)*V0)**2
           altw= U(5)*R0 - re
           W = mslug*g
           Fc = mslug*( ( (U(1)*V0)**2 ) / (U(5)*R0) )
           Tx=Thrust*DCOS(U(2))
           Ty=Thrust*DSIN(U(2))
           TPM=Thrust/mslug
            if (try .lt. 1.0d0) write(*,*) 'TPM=',TPM
            try=5.0d0
C
C..... PAR(1) -  body flap deflection
C..... q0 - Pitch rate due to spherical Earth in body axis system
C..... Note all angles are in radians EXCEPT the body flap deflection
C..... ( df=PAR(1) ) which is in degrees, therefore PAR(1) is multiplied
C..... by 2*pi/360 [rad/deg]
C
       q0 =  -(U(1) * V0)/(U(5) * R0)
*        U0 = DSQRT( g*U(5)*R0/((rho*U(5)*R0*Cl/2.0D0*mslug)+1.0D0))
       df = PAR(1) - PAR(2)*(U(3)-q0)
       CM = CM0+CMa*U(2)+CMq*(U(3)-q0)+CMdf*raddeg*df
C
      RETURN
      END
       subroutine BCND
       return
       end
       subroutine ICND
       return
       end
       subroutine FOPT
       return
       end
```

Appendix B: Standard Atmospheric Approximations for Density and Pressure

The value of density for the Standard Atmosphere (14) is calculated using a different equation over two altitude regions. The first altitude range is from 0 to 600,000 ft. The density-altitude approximation for this range was obtained directly from the work by Vihn and Dobrzelecki (15:25) and provides values of density accurate to within 5% of the Standard Atmosphere for altitudes ranging from 0 to 200 Km (0 to 656,000 ft) (15:25). This equation is an inverse polynomial relationship given by:

$$\rho = \frac{\rho_{sl}}{[A_0 + A_1 Z + \ldots + A_{11} Z^{11}]^4} \qquad (41)$$

where: ρ = density [kg m^{-3}]
ρ_{sl} = sea level density [kg m^{-3}]
Z = altitude above standard geoid (6371.315 km)
(note this is the average radius of the Earth at the equator, which is different for reference 15)
A_j = Coefficients (j=1-11) [km^{-3}]

Table 2

Coefficients for Density Polynomial

j	A_j
0	0.1000000000 E 01
1	0.3383495800 E-01
2	-0.3433553057 E-02
3	0.5497466428 E-03
4	-0.3228258326 E-04
5	0.1106607734 E-05
6	-0.2291755793 E-07
7	0.2902146443 E-09
8	-0.2230070938 E-10
9	0.1010575266 E-13
10	-0.2482089627 E-16
11	0.2548769715 E-19

(15:26)

Note the density is computed in [kg m^{-3}] and is then converted to [slugs ft^{-3}] using 1.9403232735 E-03 [(kg m^{-3})/(slugs ft^{-3})].

For altitudes above 600,000 ft the following exponential relation is used:

$$\rho = 2.16871253724E\text{-}10 \exp(-8.89837671693E\text{-}06\ Z) \qquad (42)$$

where: ρ = density [slugs ft^{-3}]
Z = altitude [ft]

Note this equation yields the value of ρ in [slugs ft^{-3}].

Figure 44 shows the calculated density relative to the Standard Atmospheric data from reference 14.

For the pressure altitude relation an exponential relationship was developed using the nonlinear fitting routine on MATLAB from MathWorks.

$$P = P0\ Exp(P1\ Z^{P2}) + P3\ Exp(P4\ Z) + P5\ Exp(P6\ Z) \qquad (43)$$

where: P = atmospheric pressure [lb ft^{-2}]
P0 = 2116.22 [lb ft^{-2}]
P1 = -5.850746831820396 E-05
P2 = 9.792179784448163 E-01
P3 = 9.875326461241002 E-05 [lb ft^{-2}]
P4 = -6.044333173347913 E-06
P5 = 3.408653276857509 E-09 [lb ft^{-2}]
P6 = -8.934489792146698 E-07
Z = equatorial altitude above the Standard geode [ft]

Figure 45 shows the quality of the pressure fit to the Standard Atmospheric data in reference 14.

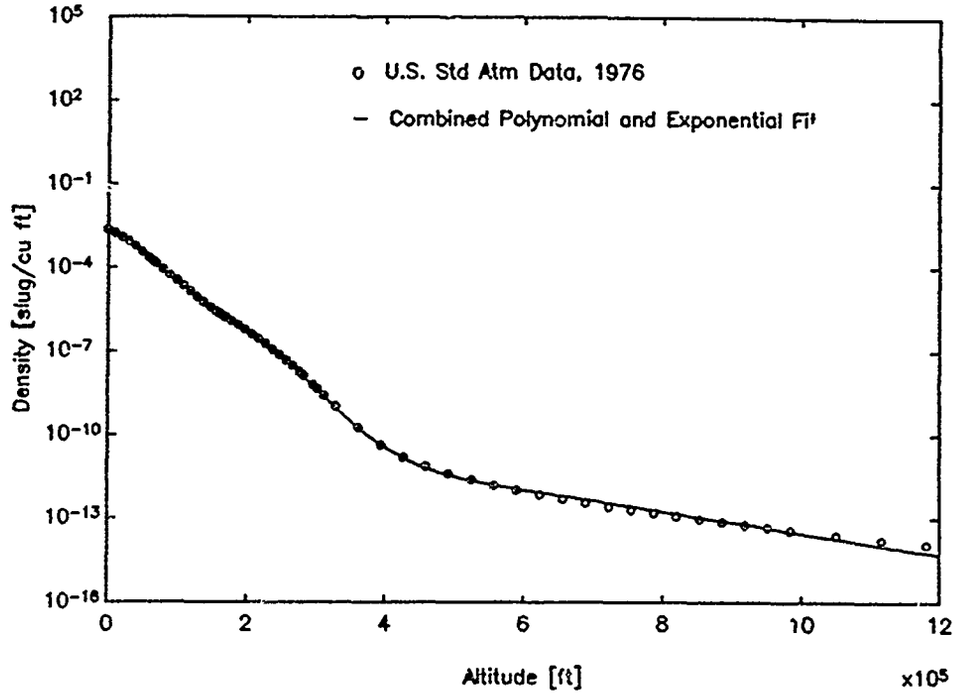

Figure 44. Comparison of Calculated Density to Standard Atmosphere

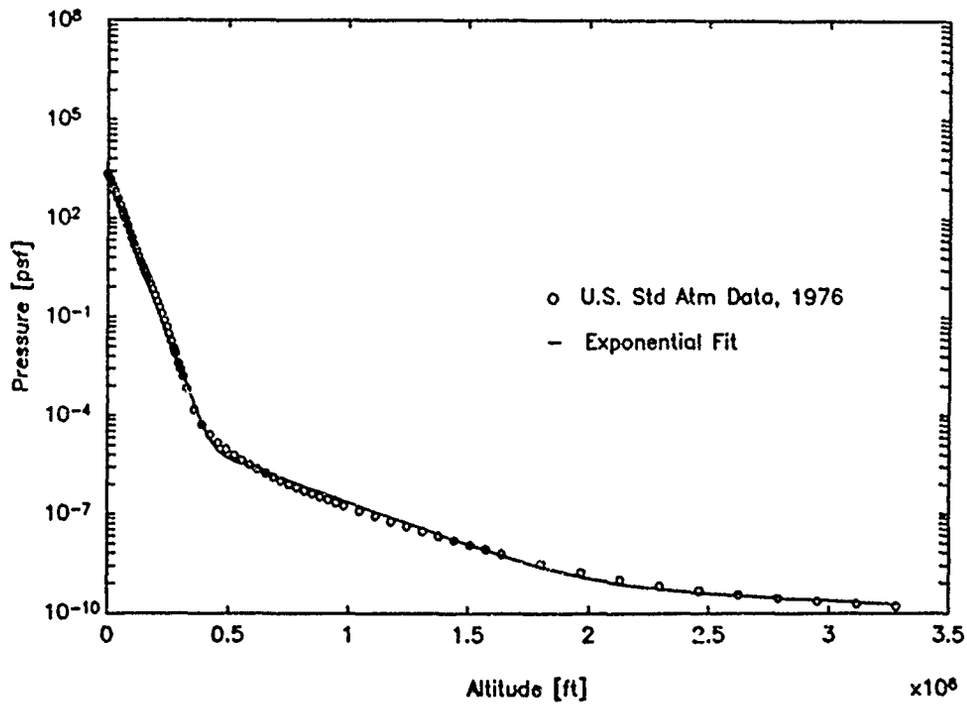

Figure 45. Comparison of Calculated Pressure with Standard Atmosphere

Bibliography

1. Anderson, John D. Jr. Hypersonic and High Temperature Gas Dynamics. New York: McGraw Hill Book Company, 1989.

2. Berry, Donald T. "Longitudinal Long-Period Dynamics of Aerospace Craft," AIAA Paper No. 88-4358-CP, AIAA Atmospheric Flight Mechanics Conference, Minneapolis, Minnesota, August 15-17, 1988.

3. Doedel, Eusebius. "AUTO: Software for Continuation and Bifurcation Problems in Ordinary Differential Equations." May 1986.

4. Etkin, Bernard. "Longitudinal Dynamics of a Lifting Vehicle in Orbital Flight," Journal of Aerospace Sciences, Vol 28, Oct. 1961, pp 779-788+.

5. Etkin, Bernard. Dynamics of Atmospheric Flight. New York: John Wiley & Sons, Inc., 1972.

6. Hill, Philip G. and Peterson, Carl R. (Third Printing) Mechanics and Thermodynamics of Propulsion. Massachusetts: Addison-Wesley Publishing Company, 1970.

7. Markopoulos, Nikos. et al. "Thrust Law Effects on the Long-Period Modes of Aerospace Craft," AIAA Paper No. 89-3379-CP.

8. McRuer, Duane. et al. Aircraft Dynamics and Control. New Jersey: Princeton University Press, 1973.

9. Neumark, S. "Longitudinal Stability, Speed and Height," Aircraft Engineering, Vol 22, pp 323-334, Nov. 1950.

10. Planeaux, James, Personal Conversations and Thesis Critique, School of Engineering, Air Force Institute of Technology (AU), Wright-Patterson AFB OH, July-December 1990.

11. Roberson, Robert E. "Gravitational Torque on a Satellite Vehicle," Journal of The Franklin Institute, Vol 265, No. 1, pp 13-22, Jan. 1958.

12. Seydel, Rüdiger. From Equilibrium to Chaos Practical Bifurcation and Stability Analysis. New York: Elsevier Science Publishing Co, Inc., 1988.

13. Stengel, Robert F. "Altitude Stability in Supersonic Cruising Flight," Journal of Aircraft, Vol 7, No. 9, pp 464-473, Sept.-Oct. 1970.

14. U.S. Standard Atmospheric 1976, prepared under sponsorship of NASA, NOAA, and USAF.

15. Vihn, Nguyen X. and Dobrzelecki, Arthur J. "Non-Linear Longitudinal Dynamics of an Orbital Lifting Vehicle," NASA CR-1449.

16. Vihn, Nguyen X. et al. Hypersonic and Planetary Entry Flight Mechanics. Michigan: University of Michigan Press, 1980.

REPORT DOCUMENTATION PAGE

Form Approved
OMB No. 0704-0188

Public reporting burden for this collection of information is estimated to average 1 hour per response, including the time for reviewing instructions, searching existing data sources, gathering and maintaining the data needed, and completing and reviewing the collection of information. Send comments regarding this burden estimate or any other aspect of this collection of information, including suggestions for reducing this burden, to Washington Headquarters Services, Directorate for information Operations and Reports, 1215 Jefferson Davis Highway, Suite 1204, Arlington, VA 22202-4302, and to the Office of Management and Budget, Paperwork Reduction Project (0704-0188), Washington DC 20503

1. AGENCY USE ONLY (Leave blank)	2. REPORT DATE	3. REPORT TYPE AND DATES COVERED
	December 1990	Master's Thesis

4. TITLE AND SUBTITLE
BIFURCATION ANALYSIS OF THE LONGITUDINAL DYNAMICS OF A SIMPLE POWERED LIFTING HYPERSONIC VEHICLE

5. FUNDING NUMBERS

6. AUTHOR(S)
Eric E. Fox, Captain, USAF

7. PERFORMING ORGANIZATION NAME(S) AND ADDRESS(ES)
Air Force Institute of Technology , WPAFB OH 45433-6583

8. PERFORMING ORGANIZATION REPORT NUMBER
AFIT/GAE/ENY/90D-07

9. SPONSORING/MONITORING AGENCY NAME(S) AND ADDRESS(ES)

10. SPONSORING MONITORING AGENCY REPORT NUMBER

11. SUPPLEMENTARY NOTES

12a. DISTRIBUTION/AVAILABILITY STATEMENT
Approved for public release; distribution unlimited

12b. DISTRIBUTION CODE

13. ABSTRACT (Maximum 200 words)

Bifurcation analysis was used to investigate the nonlinear behavior of a simple powered lifting hypersonic vehicle in circular orbit about a spherical nonrotating Earth with gradients in atmospheric density and pressure and an inverse square law for gravity. Vehicle motion is constrained to a vertical plane so only longitudinal dynamics were modeled. Bifurcation analysis was conducted using the AUTO software package. A simple five-state model with three different thrust laws was derived to describe an unaugmented vehicle whose geometric and aerodynamic characteristics follow those of the literature. A parameter representing a body flap deflection was used to conduct one set of bifurcation sweeps for each thrust law. A second set of bifurcation sweeps for each thrust law was obtained using a parameter representing a throttle which scaled the thrust. Secondary parameters representing simple feedback gains were subsequently added. Results were surprising for a simple system with basically linear aerodynamics. Periodic branches arising from the loss of pitch stability or associated with a "resonance altitude" are routinely found with significant amplitude, and periods on the order of an elliptical orbit's period for a given geocentric radius. Rotational states generally had sub-oscillations of greater frequency.

14. SUBJECT TERMS	15. NUMBER OF PAGES
Bifurcation Analysis, Hypersonic Vehicles, Aerospace Craft, Aircraft, Longitudinal Dynamics, Space Vehicles, Reentry Vehicles	102
	16. PRICE CODE

17. SECURITY CLASSIFICATION OF REPORT	18. SECURITY CLASSIFICATION OF THIS PAGE	19. SECURITY CLASSIFICATION OF ABSTRACT	20. LIMITATION OF ABSTRACT
Unclassified	Unclassified	Unclassified	UL

GENERAL INSTRUCTIONS FOR COMPLETING SF 298

The Report Documentation Page (RDP) is used in announcing and cataloging reports. It is important that this information be consistent with the rest of the report, particularly the cover and title page. Instructions for filling in each block of the form follow. It is important to **stay within the lines to meet optical scanning requirements.**

Block 1. Agency Use Only (Leave Blank)

Block 2. Report Date. Full publication date including day, month, and year, if available (e.g. 1 Jan 88). Must cite at least the year.

Block 3. Type of Report and Dates Covered. State whether report is interim, final, etc. If applicable, enter inclusive report dates (e.g. 10 Jun 87 - 30 Jun 88).

Block 4. Title and Subtitle. A title is taken from the part of the report that provides the most meaningful and complete information. When a report is prepared in more than one volume, repeat the primary title, add volume number, and include subtitle for the specific volume. On classified documents enter the title classification in parentheses.

Block 5. Funding Numbers. To include contract and grant numbers; may include program element number(s), project number(s), task number(s), and work unit number(s). Use the following labels:

C	- Contract	**PR**	- Project
G	- Grant	**TA**	- Task
PE	- Program Element	**WU**	- Work Unit Accession No.

Block 6. Author(s). Name(s) of person(s) responsible for writing the report, performing the research, or credited with the content of the report. If editor or compiler, this should follow the name(s).

Block 7. Performing Organization Name(s) and Address(es). Self-explanatory.

Block 8. Performing Organization Report Number. Enter the unique alphanumeric report number(s) assigned by the organization performing the report.

Block 9. Sponsoring/Monitoring Agency Names(s) and Address(es). Self-explanatory.

Block 10. Sponsoring/Monitoring Agency. Report Number. (If known)

Block 11. Supplementary Notes. Enter information not included elsewhere such as: Prepared in cooperation with...; Trans. of ..., To be published in .... When a report is revised, include a statement whether the new report supersedes or supplements the older report.

Block 12a. Distribution/Availablity Statement. Denote public availability or limitation. Cite any availability to the public. Enter additional limitations or special markings in all capitals (e.g. NOFORN, REL, ITAR)

DOD	- See DoDD 5230.24, "Distribution Statements on Technical Documents."
DOE	- See authorities
NASA	- See Handbook NHB 2200.2.
NTIS	- Leave blank.

Block 12b. Distribution Code.

DOD	- DOD - Leave blank
DOE	- DOE - Enter DOE distribution categories from the Standard Distribution for Unclassified Scientific and Technical Reports
NASA	- NASA - Leave blank
NTIS	- NTIS - Leave blank.

Block 13. Abstract. Include a brief (Maximum 200 words) factual summary of the most significant information contained in the report.

Block 14. Subject Terms. Keywords or phrases identifying major subjects in the report.

Block 15. Number of Pages. Enter the total number of pages.

Block 16. Price Code. Enter appropriate price code (NTIS only).

Blocks 17. - 19. Security Classifications. Self-explanatory. Enter U.S. Security Classification in accordance with U.S. Security Regulations (i.e., UNCLASSIFIED). If form contains classified information, stamp classification on the top and bottom of the page.

Block 20. Limitation of Abstract. This block must be completed to assign a limitation to the abstract. Enter either UL (unlimited) or SAR (same as report). An entry in this block is necessary if the abstract is to be limited. If blank, the abstract is assumed to be unlimited.